Aerosol optical properties and direct radiative forcing based on measurements from the China Aerosol Remote Sensing Network (CARSNET) in eastern China

Huizheng Che[1*], Bing Qi[2], Hujia Zhao[1], Xiangao Xia[3,4], Thomas F. Eck[5], Philippe Goloub[6],

Oleg Dubovik[6], Victor Estelles[7], Emilio Cuevas-Agulló[8], Luc Blarel[6], Yunfei Wu[9], Jun Zhu[10],

Rongguang Du[2], Yaqiang WANG[1], Hong Wang[1], Ke Gui[1], Jie Yu[1], Yu Zheng[10], Tianze Sun[1],

Quanliang Chen[11], Guangyu Shi[12], Xiaoye Zhang[1*]

1   State Key Laboratory of Severe Weather (LASW) and Institute of Atmospheric Composition, Chinese Academy of Meteorological Sciences, CMA, Beijing, 100081, China

2   Hangzhou Meteorological Bureau, Hangzhou, 310051, China

3   Laboratory for Middle Atmosphere and Global Environment Observation (LAGEO), Institute of Atmospheric Physics, Chinese Academy of Sciences, Beijing, 100029, China

4   School of Geoscience University of Chinese Academy of Science, Beijing, 100049, China

5   Biospheric Sciences Branch, Code 923, NASA/Goddard Space Flight Center, Greenbelt, MD, USA.

6   Laboratoire d'Optique Amosphérique, Université des Sciences et Technologies de Lille, 59655, Villeneuve d'Ascq, France

7   Dept. Fisica de la Terra i Termodinamica, Universitat de Valencia, C/ Dr. Moliner 50, 46100 Burjassot, Spain

8   Centro de Investigación Atmosférica de Izaña, AEMET, 38001 Santa Cruz de Tenerife , Spain

9   Key Laboratory of Regional Climate-Environment for Temperate East Asia, Institute of Atmospheric Physics, Chinese Academy of Sciences, Beijing 100029, China

10 Collaborative Innovation Center on Forecast and Evaluation of Meteorological Disasters, Nanjing University of Information Science & Technology, Nanjing 210044, China

11 Plateau Atmospheric and Environment Key Laboratory of Sichuan Province, College of Atmospheric Sciences, Chengdu University of Information Technology, Chengdu, 610225, China

12 State Key Laboratory of Numerical Modeling for Atmospheric Sciences and Geophysical Fluid Dynamics (LASG), Institute of Atmospheric Physics, Chinese Academy of Sciences, Beijing, 100029, China

Corresponding author: chehz@cma.gov.cn & xiaoye@cma.gov.cn

Abstract

Aerosol pollution in eastern China is an unfortunate consequence of the region's rapid economic and industrial growth. Here, sunphotometer measurements from seven sites in the Yangtze River Delta (YRD) from 2011 to 2015 were used to characterize the climatology of aerosol microphysical and optical properties, calculate direct aerosol radiative forcing (DARF), and classify the aerosols based on size and absorption. Bimodal size distributions were found throughout the year, but larger volumes and effective radii of fine-mode particles occurred in June and September due to hygroscopic growth and/or cloud processing. Increases in the fine-mode in June and September caused AOD_{440nm} > 1.00 at most sites, and annual mean AOD_{440nm} values of 0.71-0.76 were found at the urban sites and 0.68 at the rural site. Unlike north China, the $AOD_{440\ nm}$ was lower in July and August (~0.40–0.60) than in January and February (0.71–0.89) due to particle dispersion associated with subtropical anticyclones in summer. Low volumes and large bandwidths of both fine- and coarse-mode aerosol size distributions occurred in July and August because of biomass burning. Single scattering albedos at 440 nm ($SSA_{440\ nm}$) from 0.91 to 0.94, indicated particles with relatively strong to moderate absorption. Strongly absorbing particles from biomass burning with a significant SSA wavelength dependence were found in July and August at most sites while coarse particles in March to May were mineral dust. Absorbing aerosols were distributed more-or-less homogeneously throughout the region with absorption aerosol optical depths at 440 nm ~0.04-0.06, but inter-site differences in the absorption Angström exponent indicate a degree of spatial heterogeneity in particle composition. The annual mean DARF was −93 ± 44 to −79 ± 39 W/m^2 at the Earth's surface and ~ −40 W/m^2 at the top of the atmosphere (for the solar zenith angle range of 50 to 80 degrees) under cloud free conditions. The fine-mode composed a major contribution of the absorbing particles in the classification scheme based on SSA, fine mode fraction, and extinction Angström exponent. This study contributes to our understanding of aerosols and regional climate/air quality, and the results will be useful for validating satellite retrievals and for improving climate models and remote sensing algorithms.

1. Introduction

Aerosols can have important effects on the Earth's climate over regional to global scales, but there are still uncertainties in the strengths and significance of these impacts (Hansen et al.2000; Solomon et al., 2007; Schwartz and Andreae, 1996). Aerosols affect the radiative balance of the Earth–atmosphere system by directly scattering and absorbing solar radiation (Charlson et al., 1992; Ackerman and Toon, 1981), and they can affect climate indirectly through aerosol–cloud interactions (Twomey et al., 1984; Albrecht et al., 1989; Li et al., 2016).

The physical and optical properties of aerosol particles determine their radiative effects, and information on these properties can be used to predict and assess global and regional changes in the Earth's climate (Eck et al., 2005; Myhre et al., 2009; IPCC, 2013; Panicker et al., 2013). Long-term, ground-based observations have contributed greatly to our understanding of the spatial variations in aerosols and their effects on the Earth's climate (Holben et al., 2001; Kaufman et al., 2002; Sanap and Pandithurai, 2014; Li et al., 2016). Ground-based monitoring networks have been established worldwide—for instance, AERONET (Aerosol Robotic Network) (Holben et al.,1998; Goloub et al., 2007), SKYNET (SKYrad Network) (Takamura et al., 2004), EARLINET (European aerosol Lidar network) (Pappalardo et al., 2014) and the GAW-PFR Network (Global Atmosphere Watch Programmer-Precision Filter Radiometers) (Wehrli, 2002; Estelles et al., 2012). In China, CARSNET (the China Aerosol Remote Sensing NETwork) and CSHNET (the Chinese Sun Hazemeter Network) were established to obtain data on aerosol optical characteristics (Che et al., 2009a, 2015b; Xin et al., 2007). High-frequency, ground-based measurements of aerosol optical properties made at these stations have improved our understanding of the sources, transport, and diurnal variations of air pollutants, and they have provide insights into the aerosols' effects on climate. Ground-based observations are also useful for the validation of satellite retrievals (Holben et al., 2017; Xie et al., 2011).

Most of the ground-based studies of the optical properties of aerosols in China have been conducted in urban regions that have been undergoing rapid economic development. Those sites typically have had high aerosol loadings and in many cases serious environmental

92 problems (Cheng et al., 2015; Pan et al., 2010; Xia et al., 2013; Wang et al., 2015; Che et al.,

93 2015a). Detailed information on aerosol optical depth (AOD), the types of aerosols, and

94 especially the size and absorption properties of ambient populations over a wide sampling of

95 regions is needed to understand the effects of aerosols on the Earth's climate and the

96 environment (Giles et al., 2011; Che et al., 2009b; Wang et al., 2010; Zhu et al., 2014). In

97 particular, the aerosol direct radiative forcing is sensitive to the aerosol radiation absorptivity

98 (Haywood and Shine, 1995). Therefore, it is important to understand the connections between

99 the aerosol types and absorption properties because that information can be used for

100 comparisons and validation of chemical transport models and satellites (Lee et al., 2010).

101 The Yangtze River Delta (YRD) region in eastern China has recently undergone rapid

102 economic growth, and the loadings of aerosols in the region can be very high during heavy

103 pollution episodes (Fu et al., 2008; Zhang et al., 2009). Studies of aerosol optical properties in

104 eastern China have contributed to our understanding of local air quality and regional climate

105 impacts (Duan and Mao, 2007; Pan et al., 2010; Ding et al., 2016). In the YRD, investigations

106 of aerosol optical properties have been conducted in Nanjing, Hefei, Shanghai, Shouxian and

107 Taihu (Zhuang et al. 2014; Li et al., 2015; Wang et al., 2015; He et al., 2012; Lee et al., 2010;

108 Cheng et al., 2015; Xia et al., 2007). Those studies mostly involved sampling at single sites

109 ~100 km apart from one other without synchronous observations, and many have been of

110 relatively short duration, and so there remains a need for more extensive ground-based

111 measurements.

112 For the present study, sampling was conducted over a period of several years to better

113 characterize the climatology of the aerosol microphysical and optical properties, including

114 aerosol absorptivity, and to improve estimates of direct aerosol radiative forcing. For these

115 studies, sun photometer measurements were made at 3 min intervals from 2011 to 2015 at

116 seven CARSNET sites (one densely populated urban site, five urban center sites in smaller

117 cities, and one rural site) ~10–40 km apart in the YRD. The dense network of ground-based

118 sun- and sky-scanning spectral radiometers improves the temporal and spatial coverage of the

119 data, and that has enabled us to capture small-scale variations in the aerosols. The results not

120 only contribute to our understanding of regional climate and local air quality impacts, but they

121 also will be useful for validation of satellite data and improving the performance of models and

122 remote sensing algorithms in the future.

123   This paper is organized as follows: Section 2 describes the sites, the methods used for

124 retrieving the aerosol optical properties and their uncertainties, and the calculation of aerosol

125 direct radiative forcing from the retrieved aerosol optical parameters. Section 3 presents the

126 aerosol microphysical properties, optical properties, and calculations of direct radiative forcing.

127 The aerosol type classification is also presented based on the aerosol optical parameters.

128 Then a brief discussion is made about the analysis of this study. Section 4 is the conclusions.

129 **2. Site descriptions, measurements and methods**

130   Figure 1 shows the locations of the seven CARSNET sites of the YRD, and detailed

131 information on the sites is included in Table 1. Hangzhou is a densely populated urban site with

132 a heavy vehicular traffic, and it is affected by various types of anthropogenic emissions. LinAn,

133 Fuyang, Jiande, Xiaoshan and Tonglu are urban center sites in smaller cities, and they are all

134 affected to varying degrees by anthropogenic activities, especially pollutants from industries

135 and agriculture. The rural site of ChunAn has a small population, and there are few industrial

136 sources nearby so the effects from local or regional pollution are relatively small.

137   Sun photometers (CE-318, Cimel Electronique, Paris, France) were installed at each of

138 the seven sites and operated from 2011 to 2015. These instruments were standardized and

139 calibrated using CARSNET reference instruments (Che et al., 2009a), which in turn were

140 periodically calibrated at Izaña, Tenerife, Spain in conjunction with the AERONET program.

141 The cloud-screened AODs (based on the work of Smirnov et al. 2000) at 340, 380, 440, 500,

142 670, 870, 1020 and 1640 nm with uncertainties less than 0.01 (Eck et al., 1999) were obtained

143 using ASTPwin software (Cimel Electronique). The water vapor expressed as precipitable

144 water in the column was derived from the 940 nm channel with uncertainties less than 10%

145 (Eck et al., 1999). Daily averages and statistical analysis were calculated for days on which

146 instantaneous AOD measurements were made more than ten times (Che et al., 2015b). The

147 extinction Angström exponent values (EAE) were calculated from AOD values at 440 and 870

148 nm.

149   Aerosol microphysical properties were retrieved from the almucantar sky irradiance

150 measurements in conjunction with measured spectral AOD, following the methods of Dubovik

151 and King (2000) and Dubovik et al. (2002, 2006). The dataset contained information on (1)

152 volume size distributions in 22 size bins for particle radii 0.05–15 μm; (2) fine and coarse mode

153 aerosol effective radii; and (3) aerosol optical properties—including the wavelength dependent

154 single-scattering albedo (SSA), the complex refractive index, the absorption AOD (AAOD), and

155 the absorption Angström exponent (AAE). For the retrieval process, the surface albedo (SA)

156 was interpolated/extrapolated to 440, 670, 870, and 1020 nm from the daily Moderate

157 Resolution Imaging Spectroradiometer (MODIS) surface reflectance product of MCD43C3

158 (https://ladsweb.modaps.eosdis.nasa.gov/). Following the procedures of Dubovik et al.

159 (2002, 2006), all particles smaller than 0.992 μm were considered fine mode particles while

160 those larger than 0.992 μm were considered coarse mode. And the effective radii for the total

161 (Reff$_t$), fine (Reff$_{fine}$) and coarse (Reff$_{coarse}$) mode aerosols are calculated as follows:

$$R_{eff} = \frac{\int_{r_{min}}^{r_{max}} r^3 \frac{dN(r)}{dlnr} dlnr}{\int_{r_{min}}^{r_{max}} r^2 \frac{dN(r)}{dlnr} dlnr} \qquad (1)$$

162

163   Where r_{min} is 0.05, 0.05, and 0.992 μm and r_{max} is 15, 0.992, and 15 μm for the total, fine

164 and coarse mode aerosols, respectively.

165   The inversion algorithm used for calculating the aerosol volume distribution (dV/lnr)

166 assumed a homogeneous distribution of non-spherical aerosol particles as in the work of

167 Dubovik (2006); this approach has been widely applied in studies of many different areas of

168 the world. The SSA was retrieved using only AOD$_{440nm}$ > 0.40 measurements to avoid the

169 large uncertainties inherent in low AOD retrievals (Dubovik et al. 2002, 2006). Real and

170 imaginary parts of refractive index at 440, 675, 870, and 1020 nm were constrained to the

171 ranges of 1.33–1.60 and 0.0005–0.50, respectively (Dubovik and King, 2000; Che et al.,

172 2015b). The complex refractive index is assumed independent of particle size. This

173   assumption is valid for fine or coarse-dominated cases, however, could cause some errors in

174   SSA and particle size retrievals for mixed aerosol scenarios (Xu and Wang, 2015; Xu et al

175   2015). The AOD, AAOD, and AAE are related to one another as shown in equations (2) and

176   (3):

$$AAOD(\lambda) = [1 - SSA(\lambda)] \times AOD(\lambda) \qquad (2)$$

$$AAE = -dln[AAOD(\lambda)]/dln(\lambda) \qquad (3)$$

179   The inversion algorithms mentioned above have been used for AERONET and CARSNET,

180   and the accuracies of the volume size distribution were 15-25% for 0.1 μm $\leq$ r $\leq$ 7.0 μm and

181   25-100% for r < 0.1 μm and r >7μm. The accuracies for both AOD and AAOD are ~0.01. The

182   errors for the total, fine and coarse mode SSA are about 0.030, 0.037 and 0.085, respectively.

183   The imaginary and real parts of the complex refractive index for the AOD at 440 nm > 0.40 and

184   a solar zenith angle > 50° have errors of ~0.0025–0.0042 and 0.04, respectively (Dubovik et

185   al., 2000; Li et al., 2015a).

186   The direct aerosol radiative forcing (DARF) values in units of W/m^2 were calculated using

187   the radiative transfer module in the AERONET inversion (García et al., 2008; 2012) under the

188   assumption of cloud-free conditions. The DARF is defined as the difference in the shortwave

189   radiative fluxes between the two energy levels including and excluding aerosol effects at the

190   Earth's surface (bottom of the atmosphere, BOA) and the top of the atmosphere (TOA) in

191   equations (4) and (5) as follows:

$$\text{DARF}_{TOA} = F_{TOA}^{\uparrow 0} - F_{TOA}^{\uparrow} \qquad (4)$$

$$\text{DARF}_{BOA} = F_{BOA}^{\downarrow} - F_{BOA}^{\downarrow 0} \qquad (5)$$

194   where F and F^0 represent the broadband fluxes with and without aerosols at BOA and TOA,

195   respectively. The arrows in these equations indicate the direction of the fluxes for the

196   downward and upward cases. Defined this way, a negative value for ΔF indicates aerosol

197   cooling effects while positive values imply warming, both at the BOA and the TOA.

198   In the radiative transfer module used here, the flux calculations accounted for absorption

199   and multiple scattering effects using the Discrete Ordinates (DISORT) approach (Stamnes et

200   al., 1988; Nakajima and Tanaka, 1988). The solar broadband fluxes from 0.2 to 4.0 μm were

201   simulated by using information on aerosol properties (size distribution, spectral AOD, SSA,

202   and phase function) obtained from the ground-based measurements. The spectral refractive

203   indices (both real and imaginary parts) were interpolated/extrapolated from the values

204   retrieved at four distinct wavelengths (440, 670, 870, 1020 nm) from the ground-based sun

205   photometers. Likewise, the spectral dependence of surface reflectance was

206   interpolated/extrapolated from surface albedo values used in the aerosol property retrieval

207   process for the same wavelengths.

208   The integrated effects of atmospheric aerosol scattering and absorption, gaseous

209   absorption, and molecular scattering and underlying surface reflection effects were evaluated

210   using the Global Atmospheric ModEl (GAME) code (Dubuisson et al., 1996; Roger et al., 2006).

211   In the GAME code, gaseous absorption (mainly H_2O, CO_2, and O_3), is calculated from the

212   correlated k-distribution (Lacis and Oinas, 1991). The instantaneous column water vapor

213   content was retrieved by the absorption differential method from the 0.94 mm channel

214   (Smirnov et al., 2004). The total ozone content was taken from monthly climatology values

215   based on the Total Ozone Mapping Spectrometer (TOMS) measurements. The GAME model

216   accounts for spectral gaseous absorption; that is, ozone in the ultraviolet-visible spectral range

217   (0.20–0.35 μm and 0.5–0.7 μm) and water vapor in the shortwave infrared spectrum (0.8–3.0

218   μm).

219   The flux calculations were performed for a multi-layered atmosphere with the US standard

220   1976 atmosphere model for gaseous distributions and single fixed aerosol vertical distribution

221   (exponential with an aerosol height of 1 km) (Gacia et al., 2008). As these authors have

222   pointed out, solar fluxes calculated using the module described above show excellent

223   agreement with ground-based measurements of solar radiation (slope of 0.98 ± 0.00 and bias

224   of -5.32 ± 1.00 W/m^2) with a correlation of 99%. There is a small overestimation of +9 ± 12

225   Wm^{-2} of the observed solar radiation at the surface in global terms, and this corresponds to a

226   relative error of +2.1 ± 3.0%. The differences range from +14 ± 10 Wm^{-2} to +6 ± 13 Wm^{-2} for

227   urban-industrial and biomass burning aerosols, respectively. The errors are expected to be of

228   the same magnitude at the TOA, since the same methodology and inputs are used at both

229   levels (gaseous and aerosol distribution, radiative model, etc).

230   **3. Results and discussion**

231   **3.1 Aerosol microphysical properties: particle radius and volume size distributions**

232   Figure 2 shows the monthly aerosol size distribution (dV/dln$r$) for all seven sites in the

233   YRD. The annual mean values for the effective radii of the total particles (R$_{efft}$) were ~0.30 μm,

234   and the average annual volume was ~0.18 μm^3/μm^2 (Table 1). The fine-mode effective radii

235   averaged ~0.16 μm in the YRD with a fractional volume of 0.10–0.11 μm^3/μm^2 while the

236   coarse-mode average effective radii were ~2.2 μm with a fractional volume ~0.08 μm^3/μm^2.

237   These results show that there was a larger contribution of fine-mode particles to the aerosol

238   volume compared with the coarse mode at all sites. The total and fine-mode aerosol volumes

239   and effective radii showed small differences from the densely populated urban site (Hangzhou),

240   to the urban center sites in smaller cities (Xiaoshan, Fuyang, LinAn, Tonglu, Jiande) or the

241   rural site (ChunAn), and this reflects a generally homogeneous distribution of the aerosol in the

242   YRD. The coarse-mode aerosol volumes also showed small differences among site, but the

243   range of effective radii varied 2.16–2.30 μm.

244   Higher volumes and larger effective radii of the fine-mode were observed in June and

245   September at most sites, and again there were relatively small differences among sites; the

246   exception was Xiaoshan where the month-to-month differences in these variables were less

247   pronounced (Fig. 2). The increases in submicron particles during the summer may have been

248   caused in part by the hygroscopicity of the aerosols. In this regard, Saha et al. (2004) reported

249   the volume of accumulation mode particles increased faster than the coarse-mode under high

250   relative humidity conditions. At our sites, the precipitation in June and September was greater

251   than in the other months because of the "Meiyu flood period" and the "typhoon and autumn

252   rain period", respectively. Indeed, the major aerosol components, which include sulfate, nitrate,

253 ammonium, and organic compounds, can cause severe haze-fog events during high relative

254 humidity conditions. Fine particles containing sulfate, nitrate, and ammonium are hygroscopic,

255 and their sizes are strongly affected by the relative humidity (Fu et al., 2008; Shen et al., 2015;

256 Li et al., 2015b; Huang et al., 2016). Additionally, broad fine-mode distributions may result from

257 the occurrence of fog or low-altitude cloud dissipation events (Eck et al. 2012; Li et al., 2010,

258 2014). Eck et al. (2012) also pointed out that a large range of fine-mode aerosol sizes may

259 result from cloud processing, and that also could contribute to a shoulder of larger size

260 particles in the accumulation mode, especially in regions where sulfate and other

261 water-soluble aerosols exist. Another interesting observation is that the fine-mode aerosol

262 volume in July was relatively low at all sites, and is coincident with lower relative humidity in

263 July (~60%) compared with that in June (~80%) in the YRD. Therefore, the hygroscopic

264 effects on fine particles in July evidently are not as obvious as in June or September.

265 High volumes for coarse-mode aerosol occurred in March to May at all sites, and this

266 suggests that more large particles occurred in spring than in the other seasons. The most

267 likely explanation for this is the presence of mineral dust in the YRD region at that time of year.

268 High PM_{10} mass concentrations of Hangzhou during 2012-2015 showed 78.5 ± 15.4, 84.7 ±

269 11.3, and 83.6 ± 15.5 µg/m^3 in March, April, and May, respectively (see the supplement), which

270 is consistent to the results of relative large coarse-mode aerosol volumes in this study. As Cao

271 et al. (2009) pointed out, fugitive dust can account for about one-third of PM_{10} mass

272 concentration in Hangzhou, and that mainly came from re-suspended road dust and

273 construction soil. The long-range transportation of dust in spring from northern/northwestern

274 China could also contribute to the high coarse-mode aerosol volume. For instance, Fu et al.

275 (2014) and Sun et al. (2017) found that dust particles could be transported long distances, and

276 the impacts were apparent in the YRD. Low volumes and large bandwidths of coarse-mode

277 aerosol were found in July and August at all sites, and that may have been due to the wet

278 removal of coarse particles by the heavy precipitation in June. In July and August, strong

279 convection associated with subtropical anticyclone can disperse the aerosol. These results

280 also are consistent with previous reports showing minimum PM_{10} concentrations in summer of

281 the YRD region (Cao et al., 2009). It was found the PM_{10} mass concentrations of Hangzhou

282 during 2012-2015 were relative low with values 53.2 ± 6.8, and 56.7 ± 4.4 µg/m^3 in July and

283 August, respectively (see the supplement) Sun et al. (2013) found that aerosol size

284 distributions can broaden under unstable weather conditions, and in July and August, the

285 Weather in the YRD can become unstable due to the high temperatures, and this could be

286 another factor that contributed to the large bandwidth of both fine- and coarse-mode particles

287 in our study. However, these possible connections should be re-visited in the future.

288 **3.2 Aerosol optical properties: AOD and EAE**

289 The arithmetic mean annual values for AOD_{440nm} at the six urban sites (Hangzhou,

290 Xiaoshan, Fuyang, LinAn, Tonglu, Jiande) were 0.71-0.76 and 0.68 at the rural site of ChunAn

291 (Table 1). The difference in AOD between urban and rural sites was <10%, and this indicates

292 there were widespread anthropogenic impacts on the aerosol populations in the YRD and that

293 the high particle concentrations extend beyond the local to the regional scale. Nonetheless,

294 the AOD_{440nm} generally decreased from the east coast to inland areas towards the west (0.76

295 at Hangzhou, 0.73 at LinAn, 0.71 at Jiande, and 0.68 at ChunAn), and this can be explained by

296 stronger anthropogenic impacts in the more urbanized east. The high AOD_{440nm} at Hangzhou

297 was likely the result of the greater industrial activity and higher population density in the

298 eastern part of that metropolitan region; both of those factors could lead to larger aerosol

299 emissions compared with the less populated urban and rural sites. The coarse-mode AOD

300 values were just ~0.06 to 0.08, and ratios of the fine-mode $AOD_{440\ nm}$ to the total $AOD_{440\ nm}$

301 varies from 0.89-0.91 at the sites, and therefore, fine-mode particles clearly were the main

302 contributors to light extinction in the region. The less coarse mode fraction of total aerosol

303 extinction (~10%) indicated that the contribution of coarse particles to aerosol loading in the

304 YRD region is not as obvious as in other north/northeast China region (Zhang et al., 2012).

305   Table1.Geographical location and annual arithmetic mean optical parameters for aerosols from seven sites in the Yangtze River Delta.

	Hangzhou	Xiaoshan	Fuyang	LinAn	Tonglu	Jiande	ChunAn
Site type	Urban	Suburban	Suburban	Suburban	Suburban	Suburban	Rural
Longitude (°E)	120.19	120.25	119.95	119.72	119.64	119.27	119.05
Latitude (°N)	30.26	30.16	30.07	30.23	29.80	29.49	29.61
Altitude (m)	41.9	14.0	17.0	139	46.1	88.9	171.4
[a]N_{day}	485	180	217	562	498	480	439
[b]$N_{inst.}$	2052	752	906	2410	2255	1952	1731
[c]AOD_{440nm}	0.76±0.42	0.76±0.43	0.76±0.45	0.73±0.44	0.71±0.41	0.73±0.40	0.68±0.38
[c]$AOD_{fine(440nm)}$	0.68±0.42	0.69±0.41	0.69±0.44	0.66±0.43	0.64±0.41	0.66±0.40	0.61±0.38
[c]$AOD_{coarse(440nm)}$	0.08±0.06	0.07±0.06	0.07±0.06	0.07±0.07	0.07±0.06	0.07±0.07	0.06±0.05
[d]$EAE_{440-870\ nm}$	1.29±0.26	1.37±0.24	1.32±0.24	1.29±0.27	1.30±0.26	1.32±0.28	1.22±0.25
[c]SSA_{440nm}	0.91±0.06	0.93±0.04	0.94±0.04	0.93±0.05	0.92±0.04	0.92±0.05	0.94±0.03
[e]SSA_{670nm}	0.92±0.06	0.91±0.06	0.93±0.06	0.92±0.05	0.93±0.05	0.92±0.07	0.94±0.03
[f]SSA_{870nm}	0.90±0.07	0.90±0.07	0.91±0.08	0.91±0.06	0.91±0.06	0.90±0.08	0.93±0.04
[g]SSA_{1020nm}	0.89±0.08	0.89±0.08	0.89±0.09	0.90±0.07	0.90±0.07	0.90±0.09	0.92±0.05
[c]$AAOD_{440\ nm}$	0.06±0.05	0.05±0.04	0.04±0.04	0.05±0.04	0.05±0.04	0.06±0.04	0.04±0.03
[d]$AAE_{440-870\ nm}$	1.13±0.46	0.88±0.42	0.85±0.43	0.98±0.35	1.11±0.49	1.16±0.44	0.93±0.31
[c]$Reff_t(\mu m)$	0.30±0.10	0.29±0.09	0.30±0.09	0.29±0.10	0.29±0.10	0.29±0.09	0.30±0.10
[c]$Reff_{fine}(\mu m)$	0.16±0.04	0.16±0.03	0.17±0.04	0.16±0.04	0.16±0.04	0.17±0.04	0.17±0.04
[c]$Reff_{coarse}(\mu m)$	2.21±0.40	2.26±0.35	2.30±0.39	2.24±0.44	2.19±0.41	2.16±0.39	2.27±0.42
[c]$Volume(\mu m^3/\mu m^2)$	0.19±0.09	0.19±0.09	0.19±0.09	0.18±0.09	0.17±0.09	0.18±0.09	0.17±0.07
[c]$Volume_{fine}(\mu m^3/\mu m^2)$	0.10±0.06	0.11±0.06	0.11±0.07	0.10±0.06	0.10±0.06	0.10±0.06	0.10±0.06
[c]$Volume_{coarse}(\mu m^3/\mu m^2)$	0.09±0.06	0.08±0.05	0.08±0.06	0.08±0.05	0.08±0.06	0.08±0.07	0.07±0.05
[c]$DARF-BOT(W/m^2)$	−93±44	−84±41	−80±40	−81±39	−79±39	−82±40	−74±34
[c]$DARF-TOA(W/m^2)$	−35±20	−36±21	−37±21	−36±21	−35±20	−35±21	−40±19

306   Table 1 (Continued)

307   [a] Number of available observation days.

308   [b] Number of instantaneous observations.

309   [c] Optical parameters at a wavelength of 440 nm.

310   [d] Angström exponents between 440 and 870 nm.

311   [e] Optical parameters at a wavelength of 670 nm.

312   [f] Optical parameters at a wavelength of 870 nm.

313   [g] Optical parameters at a wavelength of 1020 nm.

314

315   Unlike one peak $AOD_{440\ nm}$ distribution found in June–August over northern and

316   northeastern China (Che et al., 2015), the monthly averaged AODs at 440 nm at all seven

317   sites showed two peaks, one in June and the other in September (Fig.3) with mean values of

318   ~1.26 ± 0.50 (FMF ~ 0.93) and ~1.03 ± 0.57 (FMF ~ 0.95), respectively. The FMF is defined

319   as the fine mode particle AOD_{440nm} fraction ($AOD_{fine(440nm)}/AOD_{440nm}$). Low $AOD_{440\ nm}$ values

320   of ~0.40 - 0.60 were found in July and August throughout the region, and these low values are

321   consistent with the discussion above concerning aerosol microphysical characteristics. That is,

322   hygroscopic effects and/or cloud processing of fine-mode aerosol particles caused greater

323   extinction in June and September compared with July and August. Zhang et al. (2015)

324   reported the hygroscopic particles under high relative humidity conditions could cause strong

325   aerosol light scattering in the Yangtze River Delta. Other meteorological factors also may have

326   played a role in the variations in $AOD_{440\ nm}$ during summer because in July and August,

327   subtropical high-pressure systems prevail, and the planetary boundary layer (PBLH) at

328   Hangzhou is deep, ~1.5–2.0 km (Sun et al., 2017). The large PBLH associated with

329   subtropical anticyclone favor aerosol dispersion, and this can help explain the relatively low

330   aerosol extinction observed in July and August. In January and February, high $AOD_{440\ nm}$

331   values (0.71-0.89) were observed at all sites, and this can be attributed to emissions from

332   residential heating and the stability of the atmosphere, which can cause the near surface

333   accumulation of aerosol particles. The high $AOD_{440\ nm}$ values in winter also are consistent with

334   studies by Cao et al. (2009) who reported that the PM_{10} mass concentrations at Hangzhou

335   were highest in winter. According to the PM_{10} mass concentration measurements during

336   2012-2015 at Hangzhou, it was found that the PM_{10} mass concentrations was about 82.2 ± 9.5,

337   59.1 ± 6.0, 82.8 ± 13.9, and 92.3 ± 14.3 $\mu g/m^3$ in spring, summer, autumn, and winter,

338   respectively (see the supplement).

339   The extinction Angström exponent (EAE = $-d\ln[EAOD(\lambda)]/d\ln(\lambda)$) can be regarded as an

340   indicator of aerosol size; that is, $EAE_{440\ nm-870\ nm} > 1.00$ typically indicates that the aerosol

341   particles are small. The mean extinction Angström exponent at all seven CARSNET sites was

342   higher than 1.20 throughout the year (Table 1), which means that small particles were

343   predominant. This finding is consistent with the reported dominance of small particles from

344   anthropogenic emissions and agricultural activity in the region (Tan et al., 2009).

345   **3.3 Aerosol optical properties: single-scattering albedo**

346   The SSAs at 440 nm at our seven sites in YRD region varied from 0.91 to 0.94 (Table 1),

347   and boxplots of the monthly SSAs at wavelengths of 440, 670, 870 and 1020 nm are shown in

348   Figure 4. Eck et al. (2005) reported that the SSAs at 440 nm from AERONET retrievals were

349   confined to a relatively narrow range of values globally from ~0.82 to 0.98. Therefore, the SSA

350   values in this study may be explained by moderately to strongly absorbing aerosols from

351   industrial emissions and other anthropogenic sources. The $SSA_{440\ nm}$ at Hangzhou site was

352   0.91 ± 0.06, which is lower than that at the rural ChunAn site (0.94 ± 0.03). As Dubovik et al.

353   (2000, 2002, 2006) reported, the SSA depends on two factors—particle size and composition.

354   From Table 1, one can see that the differences in effective radii for total, fine and coarse mode

355   particles between Hangzhou and ChunAn are quite small, and therefore, the differences in

356   SSAs between the two sites can best be explained by differences in composition. Furthermore,

357   the differences in SSAs between these sites indicate that there was a higher percentage of

358   absorbing aerosols at urban site than the rural one.

359   The SSAs for seven sites showed significant month-to-month variations. The increased

360   scattering (light-absorbing) effects seen in June can be attributed to hygroscopic growth, which

361   can modify aerosol properties greatly (Xia et al., 2007). The presence of light-absorbing dust

362   aerosols in spring and absorbing aerosols from biomass burning in August were probably

363   responsible for the differences in SSA values observed between those months because of the

364   distinct differences in the intensive optical properties of dust and biomass burning products

365   (Yang et al., 2009). At Hangzhou, the monthly average SSA values at 440 nm were relatively

366   high in February (~0.94 ± 0.05) and June (~0.92 ± 0.06) and more moderate in March (~0.90 ±

367   0.06) and August (~0.89 ± 0.09). In comparison, the differences in monthly SSA values at the

368   rural ChunAn site were smaller, only varying from 0.92 to 0.95. We conclude from the temporal

369   patterns of the SSAs that the types of aerosols at the urban/suburban sites were more variable

370   than at the rural sites.

371   The SSA wavelength dependence is a function of the specific absorption/scattering

372 properties of different aerosol types (Sokolik and Toon, 1999; Eck et al., 2010). The SSA for

373 mineral dust particles typically shows a strong wavelength dependence from 440 to 1020 nm

374 with a low value at 440 nm due to iron oxide absorption (Cheng et al., 2006; Dubovik et al.,

375 2002). In spring, especially in March, the SSA was obviously lower at shorter wavelengths than

376 at the longer ones, and this implies absorption by dust particles. This conclusion is consistent

377 with the discussion above concerning the impact of dust on aerosol size distributions. In

378 addition, there was a significant decrease in SSA at shorter wavelengths in July and August at

379 most sites, and this supports the presence of aerosol particles with strong absorption,

380 especially at infrared wavelengths. The decreases in those months can be explained by

381 strongly absorbing aerosols from biomass burning or possibly industrial emissions. As Ding et

382 al. (2013a, b) and Wang and Zhang (2008) have reported, plumes from agricultural burning

383 typically contain light-absorbing carbonaceous aerosols, and these pollutants can seriously

384 impair air quality. Indeed, aerosols from biomass burning were more than likely responsible for

385 the low in SSAs found in our study during July and August.

386 **3.4 Aerosol optical properties: AAOD and AAE**

387   The AAODs at 440 nm at the seven sites were similar ~ 0.04-0.06 (Fig. 5a and Table 1),

388 and therefore, absorbing aerosols apparently were widely distributed throughout the YRD.

389 There were large uncertainties in the $AAOD_{440\ nm}$, however; in fact, the standard deviations

390 (0.03 to 0.05) were comparable to the means, and this reflects the large temporal variability in

391 absorbing aerosol particle loadings. The average $AAOD_{440\ nm}$ at Hangzhou was about 0.02

392 higher than that at ChunAn, and this shows that the relative proportion of absorbing particles at

393 the urban area was larger than at the rural site, presumably due to greater anthropogenic

394 emissions. From Fig. 5, one can see that the monthly $AAOD_{440\ nm}$ at the urban sites from

395 March to November usually exceeded 0.05, which implies there were more absorbing species

396 in spring and autumn compared with winter (December to February) when the $AAOD_{440\ nm}$

397 tended to be lower, < 0.05. This result suggests that the relative abundances of light-absorbing

398 particles were lower in winter compared with other seasons, and this is different from many

399 regions in northern China where the AAODs are highest in winter due to the emission of

400 absorbing particles from residential heating and other sources (Zhao et al., 2015). At the

401 ChunAn, the variations in AAODs were smoother than the more heavily impacted urban sites,

402 and the monthly mean AAODs at ChunAn were < 0.05 throughout the year.

403   The AAE can be viewed as an indicator of the type of dominant absorbing aerosol

404 particles, which include black carbon, organic matter, and mineral dust (Giles et al., 2012).

405 Generally, an AAE < 1 indicates mixing, coating, and coagulation of black carbon with organic

406 and inorganic materials; an AAE close to 1 indicates absorbing black carbon aerosols from the

407 fossil fuel burning; and an AAE >1.10 indicates absorbing aerosols mainly from the biomass

408 burning or mineral dust (Russell et al., 2010; Bergstrom et al., 2007; Lack and Cappa, 2010).

409 The annual mean AAEs at Hangzhou, Xiaoshan, Fuyang, LinAn, Tonglu, Jiande and ChunAn

410 were 1.13 ± 0.46, 0.88 ± 0.42, 0.85 ± 0.43, 0.98 ± 0.35, 1.11 ± 0.49, 1.16 ± 0.44 and 0.93 ±

411 0.31, respectively (Table 1), and for discussion purposes, the seven sites were grouped into

412 three categories based on their average AAEs. The mean AAE values at Xiaoshan and

413 Fuyang were < 1.00, which suggests that coated black carbon particles dominated at these

414 two sites. However, this also could be due to measurement uncertainties due to smaller

415 numbers of samples from those sites or to slightly larger values of the imaginary part of the

416 refractive index at longer wavelengths for certain particles (Bergstrom et al., 2007). There

417 would need to more observations to confirm the low AAEs at these two sites.

418   The AAE values ~1.00 at LinAn and ChunAn indicate that the absorbing aerosol

419 population was mainly composed of black carbon from fossil fuel burning. LinAn has a more

420 developed economy compared with Tonglu and Jiande, and in comparison, LinAn has many

421 more motor vehicles and is more heavily impacted by industrial emissions and fossil fuel

422 combustion. In contrast, the ChunAn site is located in the Qiandao Lake National Water

423 Resources Protection Zone where biomass burning and industrial activities are banned. Thus,

424 emissions from motor vehicles are probably the main source of absorbing carbon aerosols at

425 ChunAn. Finally, the AAE values at Hangzhou, Tonglu and Jiande were > 1.10, indicating a

426 predominance of light-absorbing aerosols from either biomass burning or mineral dust.

427   Hangzhou has a population of ~10 million and more than one million vehicles, and the city can

428   be impacted by fugitive dust and biomass burning emissions (Cao et al., 2009). Tonglu and

429   Jiande have small economies compared with Hangzhou, but there is more agricultural

430   production near those two sites, and they can be impacted by biomass burning. These

431   inter-site differences in the AAEs reflect a degree of spatial heterogeneity in the distributions of

432   absorbing aerosols even though the AODs were relatively similar, and these differences likely

433   result from the many types of emission sources that can impact the sites.

434   **3.5 Direct Aerosol radiative forcing at the Earth's surface and TOA**

435   In this study, only clear sky direct aerosol radiative forcings could investigated because

436   the aerosol microphysical and optical parameters were derived from ground-based retrievals

437   under free cloud conditions. For the direct aerosol radiative forcing calculations, the solar

438   fluxes are only evaluated for solar zenith angles (SZA) between 50º and 80º, which is where

439   the solar geometry conditions are the most appropriate for retrieving the aerosol properties

440   (Dubovik et al., 2000, 2002).

441   The annual direct DARF-BOA values under clear conditions for Hangzhou, Xiaoshan,

442   Fuyang, LinAn, Tonglu, Jiande and ChunAn were −93 ± 44, −84 ± 40, −80 ± 40, −81 ± 39, −79

443   ± 39, −82 ± 40 and −74 ± 34 W/m^2, respectively (Figure 6a). The DARF-BOA at Hangzhou was

444   ~ −20 W/m^2 lower than that at the rural ChunAn site. The DARFs at the Earth's surface and

445   TOA are governed by the aerosol microphysical and optical properties, primarily particle size

446   distributions, AODs and SSAs. The large negative DARF-BOA values at Hangzhou can be

447   attributed to the high aerosol extinction (AOD$_{440\ nm}$ ~ 0.76) and small absorption (SSA at 440

448   nm ~0.91). These calculations indicate that effects of those particles on radiative fluxes can

449   cause significant surface cooling at that urban site. In comparison, at the rural ChunAn site,

450   less negative DARF-BOA values result from lower aerosol extinction (AOD$_{440\ nm}$ ~ 0.68) and

451   higher scattering (SSA$_{440\ nm}$ ~ 0.94).

452   The monthly DARF-BOA at the seven sites was most strongly negative in June, followed

453   by March and September. The strong cooling effect at the surface in June was due to the high

454   aerosol extinction (in section 3.2) and in particular the high volumes of fine-mode particles as

455 shown in Fig.2. Weakly absorbing particles with $SSA_{440\,nm}$ ~0.90-0.95 (Fig.6) also would

456 reduce the flux of solar radiation to the surface. A large surface cooling effect also was found in

457 March and April. Although the AOD in spring was lower than in winter, there were more

458 strongly absorbing aerosols with relatively smaller SSAs at shorter wavelengths then, and this

459 can be attributed to the presence of mineral aerosol particles. These coarse mode particles

460 with high volumes and large radii are common in spring (see section 3.1), and they can absorb

461 and scatter solar radiation and in so doing cool the surface. Surface cooling in September can

462 be explained by high aerosol extinction that resulted from the high volumes of weakly

463 absorbing fine-mode particles ($SSA_{440\,nm}$ ~0.90-0.95). These results indicate that the

464 attenuation of the solar radiation by the aerosols leads to significant surface cooling over the

465 YRD.

466   The DARF-TOA annual mean values under clear conditions were ~ −40 W/m^2 at all sites

467 (Figure 7a), and these negative DARF-TOA values indicate that the aerosols caused cooling

468 whole earth-atmosphere system in the YRD. This is different from the case in

469 north/northeastern China where the instantaneous DARF-TOA value can be positive in winter

470 due to the high surface reflectance of short wavelength radiation combined with atmospheric

471 heating caused by absorbing aerosols (Zhao et al., 2015, Che et al., 2014).

472   The monthly DARF-TOA means under clear conditions varied smoothly during two

473 periods: (1) from January to May, (2) from October to December (Fig. 7). The DARF-TOA

474 values were found approximate -40 W/m^2 at all sites in above two periods. However, the

475 monthly DARF-TOA means in June and September exceeded -40 W/m^2 at most sites, which

476 indicated more cooling effects on the whole earth-atmosphere system due to large aerosol

477 extinctions in YRD. The DARF-TOA means were about −20 W/m^2 at the seven sites in

478 July/August, which suggests weak cooling at that time. In contrast, the DARF-TOA values

479 under clear conditions at Shenyang (urban area of Northeastern China), Beijing (urban area of

480 Northern China), and Xianghe (rural area of Northern China) showed the negative peak during

481 June to August due to the large aerosol extinctions in summer season (Zhao et al., 2015; Xia

482 et al., 2016). As noted in section 3.3, the SSA was low in July and August, and that was

483 attributed to absorbing particles from biomass burning. Ding et al. (2016) found that large

484 quantities of black carbon can be emitted from biomass burning in the YRD during the summer,

485 and because these particles strongly absorb at infrared wavelengths, they can cause heating

486 up the atmosphere and resulting in lower negative ARF-TOA. Indeed, the positive DARF-TOA

487 we found under clear conditions from April to October were mainly due to the effects of

488 strongly absorbing particles; that is, the SSAs at 440 nm were < 0.80, and they showed a

489 strong decrease with wavelength (not shown here) when DARF-TOA values were positive.

490 Moreover, strongly absorbing aerosol particles can heat the atmosphere column and the TOA

491 at the same time.

3.6 Aerosol type classification based on the aerosol optical properties

493 In previous studies, aerosol types have sometimes been simply classified as dust (high

494 AOD, low AE) and anthropogenic aerosols (high AOD, high AE) (Che et al., 2009a, b; Wang et

495 al., 2010). However, aerosol direct radiative forcing is affected by the absorptivity of aerosol

496 and the underlying surface conditions (Haywood and Shine, 1995), and there are advantages

497 to better characterization of the aerosol populations. For example, the classification of

498 ground-based aerosol types can be used to compare and validate aerosol types in chemical

499 transport models and satellites retrievals (Lee et al., 2010). Thus, it is advantageous to

500 categorize aerosols as absorbing or non-absorbing based on ground-based optical

501 parameters, including SSA, fine-mode fraction of AOD, and EAE etc. In this study, we used the

502 SSA, FMF, and EAE values to classify the fine and coarse mode particles from each site into

503 eight groups of particles following the method of Zheng et al. (2017). The eight types of

504 particles were (I) highly-absorbing fine-mode particles (AE > 1.2, SSA ≤ 0.85); (II)

505 moderately-absorbing fine-mode particles (AE > 1.2, 0.85 ≤ SSA < 0.9); (III) slightly-absorbing

506 fine-mode particles (AE > 1.2, 0.9 ≤ SSA < 0.95); (IV) weakly-absorbing fine-mode particles

507 (AE > 1.2, SSA > 0.95); (V) mixed-absorbing particles (0.6 ≤ AE < 1.2, SSA ≤ 0.95); (VI) mixed

508 slightly absorbing particles (0.6 ≤ AE < 1.2, SSA > 0.95); (VII) strongly absorbing coarse mode

509 particles—mainly dust (AE≤ 0.6, SSA ≤ 0.95); (VIII) weakly-absorbing coarse-mode particles

510 (AE ≤ 0.6, SSA > 0.95).

511

From Figure 8 and 9, one can see that the absorbing fine-mode particles (Type I, II and III) accounted for ~30 to 50% of the aerosol in the YRD region with the FMF ~0.86-0.94%. The percentages of "highly-absorbing fine-particles" (Type I) was obviously larger at Hangzhou (~8%) (FMF~0.90) than the smaller city sites (~2-3%), and at the ChunAn rural site, the percentages of Type I particles was only ~0.16% (FMF~0.91). This indicates that there were greater emissions of strong absorbing aerosols from sources such as biomass burning and/or urban/industrial activities at the urban site compared with the rural one. The proportion of weakly-absorbing fine-mode particles (Type IV) varied from ~20 to 30% for all sites, and the FMF varies from 0.89~0.95 at same time, which suggests the second largest aerosol type in the area is weakly-absorbing fine-mode particles. The percentage of mixed absorbing particle (Type V) was about ~25-26% both at Hangzhou and the rural ChunAn site, which is slightly higher than that at small city sites (~10-20%) where the FMF of these particles was ~0.81-0.89. The higher FMF at Hangzhou was probably due to the complex aerosol emission sources that impact that megacity while at ChunAn, which is surrounded by mountains, the basin topography promotes particle mixing. The mixed slightly absorbing particles (Type VI) showed the highest percentages of the total aerosol number at Fuyang (18.05%) and ChunAn (15.32%), and the FMF of this group varied from 0.84-0.91 at all sites. The contribution of Type VI mixed slightly absorbing particles at Hangzhou was ~11.49%, and the FMF (0.86) there was not as high as at ChunAn (0.91). The proportion of strongly absorbing coarse mode particles—mainly dust (Group VII) was only ~1.04% of the total particle count at Hangzhou while at the other sites the percent abundances were < 1%, and the FMF for these particles were ~0.50-0.63 at all sites. These patterns show that the YRD region is different from regions in north China, including Beijing, where dust particles contribute significantly to the coarse mode absorption (Zheng et al., 2017). The percentage of weakly-absorbing coarse–mode particles (Group VIII) at all sites was < 0.54%, which shows that this aerosol type was rare. In addition, the FMF of Group VIII particles was 0.5–0.8 with large uncertainties at all sites. Overall, this analysis of aerosol types shows that the aerosol absorption is relatively weak in the YRD region, and the fine-mode makes up an especially large contribution of the absorbing

540   particles at Hangzhou.

541   **3.7 Discussion**

542   Compared with previous studies on the climatology of aerosol microphysical and optical

543   properties in China, large volumes and effective radii of fine-mode aerosol, as well as high

544   AODs at 440 nm were found at most sites in June and September but not in July or August.

545   This is remarkably different from studies conducted in Northeastern/Northern China where

546   these properties showed the maximum values in July or August (Eck et al., 2005; Zhao et al.,

547   2013; Che et al., 2015b). This reflects the distinctive climatology of aerosol microphysical and

548   optical properties in the YRD region of Eastern China. This information on the distributions and

549   variations of aerosol microphysical and optical properties obtained in our study should be

550   taken into account in the validation of satellite retrievals and aerosol modeling studies in the

551   future.

552   The $AOD_{440\,nm}$ values in our study (0.71- 0.76) are similar to other urban areas of China,

553   such as Shenyang (0.75), Beijing (0.76), Tianjin (0.74), Shanghai (0.70), and Hefei (0.69) (Pan

554   et al., 2010; He et al., 2012; Zhao et al., 2013; Che et al., 2015b, Liu et al., 2017). This

555   indicates that high aerosol loadings caused by anthropogenic activities occur over many urban,

556   suburban, and even rural areas of eastern China. The $AOD_{440\,nm}$ at the rural ChunAn site

557   (~0.68) is ~ 2–6 times higher than in other rural sites in China, such as Longfengshan (0.35;

558   northeastern China), Xinglong (0.28, northern China), Akedala (0.20, northwestern China) and

559   Shangri-La (0.11, southwestern China) (Wang et al., 2010; Che et al., 2011; Zhu et al., 2014;

560   Che et al., 2015b). Therefore, strong aerosol effects on light extinction occur not only in urban

561   areas but also in much or possibly all of the YRD. The $SSA_{440\,nm}$ in our study ranged from

562   0.91–0.94, which is similar to other regions of China, such as Wuhan (0.92), Beijing (0.89) and

563   Xinglong (0.92) (Wang et al., 2015; Xin et al., 2014; Zhu et al., 2014); this suggests aerosol

564   particles in the YRD are slight to relatively strong absorbers of violet/indigo wavelengths.

565   Although the AAE has been used as an indicator of the dominant absorbing aerosol type,

566   the SSA, FMF, and EAE also used to classify the absorption characteristics of fine and coarse

567 mode particles. It should also be mentioned that uncertainties in the AAE calculations due to

568 uncertainties in the SSAs may have contributed to the observed differences between sites

569 (Bergstrom et al., 2007; Giles et al. 2011). Ideally, the aerosol physical and chemical

570 characteristic measurements will be combined at some point to more definitively classify the

571 aerosol types. In addition, even though Zhuang et al. (2017) pointed that the DARFs are not

572 very sensitive to vertical profiles under clear sky condition, future research should take into

573 account the vertical distributions of aerosols to more accurately assess the direct aerosol

574 radiative forcing effects.

575 The useful observations at most sites in this study were made on 439~562 days, but

576 smaller numbers of observation were made in Xiaoshan and Fuyang because of instrument

577 failures, 180 and 217 days, respectively. There were fewer than 15 days of useful data for

578 October and November at Fuyang, and for June, July, September, and November at

579 Xiaoshan. While the available data do provide insights into the aerosol characteristics at

580 the sites, more extended observations should be conducted at the two sites in future.

581 **4. Conclusions**

582 A detailed study of aerosol microphysical and optical properties retrieved from

583 synchronous ground-based sun photometer observations was conducted at seven sites in the

584 Yangtze River Delta region of Eastern China from 2011 to 2015. The aerosol were classified

585 into eight types, and calculations were made for the direct aerosol radiative forcing (DARF) at

586 the top and bottom of the atmosphere. The conclusions of the study can be summarized as

587 follows:

588 A relatively homogeneous distribution of aerosol microphysical properties was found for a

589 megacity, five small cities, and a rural site in the YRD region. High particle volumes of

590 coarse-mode aerosol occurred in March to May, which reflects the existence of large mineral

591 particles from springtime dust storms. High volumes and large effective radii of fine-mode

592 aerosol in June and September were found at most sites, and this was attributed to aerosol

593 hygroscopicity and cloud processing. The low volumes and large bandwidth of both fine- and

594 coarse-mode aerosol found in July and August at all sites was explained by the wet removal of

595 coarse particles during the heavy precipitation in June and the influences of subtropical

596 anticyclones in summer.

597 The $AOD_{440 nm}$ generally decreased from the east coast (0.76–Hangzhou) to the inland

598 areas towards the west (0.68–ChunAn), and this can be explained by anthropogenic impacts

599 of the more urbanized regions in the east YRD region. The $AOD_{440 nm}$ values at urban and rural

600 sites of YRD were 0.68–0.76, and the fine-mode fractions were ~0.90, which indicates that

601 fine-mode particles were more important than the coarse mode for the light extinction. The

602 difference in AODs between the urban and rural sites was less than 10%, and this can be

603 explained by somewhat stronger effects of anthropogenic activities in the urban area. The

604 monthly averaged AODs at 440 nm showed peaks in June and September that resulted from

605 increases fine-mode aerosol particles. However, AODs at 440 nm in July and August were the

606 lowest over the year, and that was related to conditions favorable for aerosol dispersion. The

607 mean extinction Angström exponent was > 1.20 all year indicating that small particles were

608 predominant in the region. The SSAs at 440 nm varied from 0.91 to 0.94 at the urban and rural

609 sites, indicating that the aerosol particles were moderately absorbing, and this is almost surely

610 a result of impacts from the high industrial emissions and other anthropogenic activities in the

611 region. There was an obvious wavelength dependence for the SSA in July and August, and

612 aerosols absorbed most strongly at infrared wavelengths. The AAODs at 440 nm at the seven

613 sites were ~0.04–0.06, which suggests that absorbing aerosols are distributed more-or-less

614 homogeneously throughout the YRD region. The averaged $AAOD_{440 nm}$ at Hangzhou is about

615 0.02 higher than that at ChunAn, which indicates the relative proportion of absorbing particles

616 in the urban area is larger compared with the rural area. The $AAOD_{440 nm}$ in winter was < 0.05,

617 which suggests that light absorption by the particles was low compared with the other seasons.

618 The geographical variability in the distributions of the AAEs suggests that the absorbing

619 aerosols possibly have different optical characteristics related to the local emission sources in

620 the YRD.

621 The DARF-BOA at Hangzhou was ~ −20 W/m^2 lower than that at the rural ChunAn site,

622 which shows stronger aerosol cooling at the megacity. The monthly DARF-BOA was strongly

623 negative in June due to the high aerosol extinction and especially the high fine-mode volume.

624 The DARF-TOAs under clear conditions were < -40 W/m^2, but about -20 W/m^2 in July/August

625 which suggests weaker cooling in mid summer. The DARF-TOAs were positive from April to

626 October when the SSA $_{440 nm}$ < 0.80, and the greater effects at shorter wavelengths was likely

627 due to emissions of carbonaceous particles from the burning of crop residues.

628 The SSA, FMF, and EAE values were used to classify the particles as absorbing or

629 non-absorbing. Relatively large emissions of strongly absorbing aerosols in the Hangzhou

630 urban area was the result of biomass burning and/or urban/industrial activities. The aerosol

631 type classification showed overall that the aerosol absorption is weak to moderate in the YRD,

632 and the fine-mode has a large contribution to the higher percentage of absorbing particles at

633 the Hangzhou site.

634 **Acknowledgments**

635 This work was supported by grant from National Key R & D Program Pilot Projects of

636 China (2016YFA0601901), National Natural Science Foundation of China (41590874,

637 41475138 & 41375153), Natural Science Foundation of Zhejiang Province (LY16010006), the

638 CAMS Basis Research Project (2016Z001 & 2014R17), the Climate Change Special Fund of

639 CMA (CCSF201504), CAMS Basic Research Project (2014R17),the Special Project of

640 Doctoral Research supported by Liaoning Provincial Meteorological Bureau (D201501),

641 Hangzhou Science and Technology Innovative project (20150533B17)and the European

642 Union Seventh Framework Programme (FP7/2007-2013) under grant agreement no. 262254.

643 The authors would like to thank the three anonymous reviewers and the editor for their

644 constructive suggestions and comments.

645 **References**

646 Ackerman, P., and Toon, O.B.: Absorption of visible radiation in atmosphere containing

647 mixtures of absorbing and nonabsorbing particles, Appl. Opt., 20, 3661-3668, 1981.

648 Albrecht, B.: Aerosols, cloud microphysics, and fractional cloudiness, Science, 245,

649   1227-1230, 1989.

650   Bergstrom, R.W., Pilewskie, P., Russell, P.B., Redemann, J., Bond, T.C., Quinn, P.K., and

651   Sierau, B.: Spectral absorption properties of atmospheric aerosols, Atmos. Chem. Phys., 7,

652   5937–5943, doi: 10.5194/ acp-7-5937-2007, 2007.

653   Cao, J., Shen, Z., Chow, J.C., Qi, G., and Watson, J.G.: Seasonal variations and sources of

654   mass and chemical composition for PM10 aerosol in Hangzhou, China, Particuology, 7, 161–

655   168, doi:10.1016/j.partic.2009.01.009, 2009.

656   Charlson, R.J., Schwartz, S.E., Hales, J.M., Cess, D., Coakley, J.A., and Hansen, J.E.:

657   Climate forcing by anthropogenic aerosols, Science, 255, 423–430, 1992.

658   Che, H.Z., Xia, X.A., Zhu, J., Wang, H., Wang, Y.Q., Sun, J.Y., Zhang, X.C., Zhang, X.Y., and

659   Shi, G.Y.: Aerosol optical properties under the condition of heavy haze over an urban site of

660   Beijing, China, Environ. Sci. Pollut. Res., 22, 1043–1053, 2015a.

661   Che, H. Z., Zhang, X. Y., Alfraro, S., Chatenet, B., Gomes, L., and Zhao, J. Q.: Aerosol optical

662   properties and its radiative forcing over Yulin, China in 2001 and 2002, Adv. Atmos. Sci., 26,

663   564–576, doi:10.1007/s00376-009-0564-4, 2009b.

664   Che, H., Zhang, X., Chen, H., Damiri, B., Goloub, P., Li, Z., Zhang, X., Wei, Y., Zhou, H., Dong,

665   F., Li, D., and Zhou, T.: Instrument calibration and aerosol optical depth (AOD) validation of the

666   China Aerosol Remote Sensing Network (CARSNET), J. Geophys. Res., 114, doi:

667   org/10.1029/2008JD011030, 2009a.

668   Che, H., Wang, Y., Sun, J., and Zhang, X.: Assessment of In-situ Langley Calibration of

669   CE-318 Sunphotometer Mt. Waliguan Observatory, China, SOLA, 7, 089-092, doi:

670   10.2151/sola.2011-023, 2011.

671   Che, H.Z., Zhang, X.Y., Xia, X.A., Goloub, P., Holben, B., Zhao, H., Wang, Y., Zhang, X.C.,

672   Wang, H., and Blarel, L. et al.: Ground-based aerosol climatology of China: Aerosol optical

673   depths from the China Aerosol Remote Sensing Network (CARSNET) 2002–2013, Atmos.

674   Chem. Phys., 15, 7619–7652, 2015b.

675   Che, H.Z., Xia, X.A., Zhu, J., Wang, H., Wang, Y.Q., Sun, J.Y., Zhang, X.C., Zhang, X.Y., and

676   Shi, G.Y.: Aerosol optical properties under the condition of heavy haze over anurban site of

677   Beijing, China, Environ. Sci. Pollut. Res.,http://dx.doi.org/10.1007/s11356-014-3415-5, 2014.

678   Cheng, T., Liu, Y., Lu, D., Xu, Y., and Li, H.: Aerosol properties and radiative forcing in

679   Hunshan Dake desert, northern China, Atmos. Environ., 40, 2169-2179, 2006.

680   Cheng, T.T., Xu, C., Duan, J.Y., Wang, Y.F., Leng, C.P., Tao, J., Che, H.Z., He, Q.S., Wu, Y.F.,

681   Zhang, R.J., Li, X., Chen, J.M., Kong, L.D., and Yu, X.N.: Seasonal variation and difference of

682   aerosol optical properties in columnar and surface atmospheres over Shanghai, Atmos.

683   Environ., 123, 315-326, 2015.

684   Ding, A. J., Fu, C. B., Yang, X. Q., Sun, J. N., Zheng, L. F., Xie, Y. N., Herrmann, E., Nie, W.,
685   Petäjä, T., Kerminen, V.-M., and Kulmala, M.: Ozone and fine particle in the western Yangtze
686   River Delta: an overview of 1 yr data at the SORPES station, Atmos. Chem. Phys., 13, 5813–
687   5830, doi:10.5194/acp-13-5813-2013, 2013a.

688   Ding, A. J., Fu, C. B., Yang, X. Q., Sun, J. N., Petäjä, T., Kerminen, V.-M., Wang, T., Xie, Y.,

689   Herrmann, E., Zheng, L. F., Nie, W., Liu, Q., Wei, X. L., and Kulmala, M.: Intense atmospheric

690   pollution modifies weather: a case of mixed biomass burning with fossil fuel combustion

691   pollution in eastern China, Atmos. Chem. Phys., 13, 10545-10554,

692   doi:10.5194/acp-13-10545-2013, 2013b.

693   Ding, A. J., Huang, X., Nie, W., Sun, J. N., Kerminen, V.M., Petäjä, T., Su, H., Cheng, Y. F.,

694   Yang, X.Q., and Wang, M.H. et al.: Enhanced haze pollution by black carbon in megacities in

695   China, Geophys. Res. Lett., 43, 2873–2879, doi: 10.1002/2016GL067745, 2016.

696   Duan, J., Mao, J.: Study on the distribution and variation trends of atmospheric aerosol optical

697   depth over the Yangtze River Delta, Acta Scien. Circum., 27 (4), 537-543, 2007.

698   Dubovik, O., Holben, B.N., Eck, T.F., Smirnov, A., Kaufman, Y.J., King, M.D., Tanre, D.,

699   Slutsker, I.: Variability of absorption and optical properties of key aerosol types observed in

700   worldwide locations, J. Atmos. Sci., 59, 590–608, 2002.

701   Dubovik, O., King, M.D.: A flexible inversion algorithm for retrieval of aerosol optical properties

702   from sun and sky radiance measurements, J. Geophys. Res., 105 (D16), 20673, 2000.

703   Dubovik, O., Sinyuk, A., Lapyonok, T., Holben, B.N., Mishchenko, M., Yang, P., Eck, T.F.,

704   Volten, H., Munoz, O., Veihelmann, B., van der Zande, W.J., Leon, J.F., Sorokin, M., and

705   Slutsker, I.: Application of spheroid models to account for aerosol particle nonsphericity in

706   remote sensing of desert dust, J. Geophys. Res.-Atmos., 111 (D11), 2006.

707   Dubovik, O., Smirnov, A., Holben, B. N., King, M. D., Kaufman, Y. J., Eck, T. F., and Slutsker, I.:

708   Accuracy assessments of aerosol optical properties retrieved from Aerosol Robotic Network

709   (AERONET) Sun and sky radiance measurements, J. Geophys. Res., 105(D8), 9791–9806,

710   2000.

711   Dubuisson, P., Buriez, J. C., and Fouquart, Y.: High spectral resolution solar radiative transfer

712   in absorbing and scattering media, application to the satellite simulation, J. Quant. Spectrosc.

713   Radiat. Transfer, 55, 1996.

714   Eck, T.F., Holben, B.N., Dubovik, O., Smirnov, A., Goloub, P., Chen, H.B., Chatenet, B., Gomes,
715   L., Zhang, X.Y., and Tsay, S.C. et al.: Columnar aerosol optical properties at AERONET sites in
716   central eastern Asia and aerosol transport to the tropical Mid-Pacific, J. Geophys. Res., 110,
717   2005.

718   Eck, T. F., Holben, B. N., Reid, J. S., Dubovik, O., Smirnov, A., O'Neill, N. T., Slutsker, I., and

719   Kinne, S.: Wavelength dependence of the optical depth of biomass burning, urban, and desert

720   dust aerosols, J. Geophys. Res., 104(D24), 31333–31349, 1999.

721   Eck, T.F., Holben, B.N., Reid, J.S., Giles, D.M., Rivas, M.A., Singh, R.P., Tripathi, S.N.,

722   Bruegge, C.J., Platnick, S., Arnold, G.T., Krotkov, N.A., Carn, S.A., Sinyuk, A., Dubovik, O.,

723   Arola, A., Schafer, J.S., Artaxo, P., Smirnov, A., Chen, H. and Goloub, P.: Fog- and Cloud

724   induced aerosol modification observed by the Aerosol Robotic Network (AERONET), J.

725   Geophys. Res., 117, D07206, doi: 10.1029/2011JD016839, 2012.

726   Eck, T. F., Holben, B. N., Sinyuk, A., Pinker, R. T., Goloub, P., Chen, H., Chatenet, B., Li, Z.,

727   Singh, R. P., and Tripathi, S. N.: Climatological aspects of the optical properties of fine/coarse

728   mode aerosol mixtures, J. Geophys. Res. Atmos. (1984–2012), 115, 19205, 2010.

729   Estellés, V., Campanelli, M., Utrillas, M. P., Expósito, F., and Martínezlozano, J. A.:

730   Comparison of AERONET and SKYRAD4.2 inversion products retrieved from a Cimel CE318

731   sunphotometer, Atmos. Meas. Tech., 4, 569-579, 2012.

732   Fu, Q., Zhuang, G., Wang, J., Xu, C., Huang, K., Li, J., Hou, B., Lu, T., and Streets, D. G.:

733   Mechanism of formation of the heaviest pollution episode ever recorded in the Yangtze River

734   Delta, China, Atmos. Environ., 42, 2023-2036, 2008.

735   Fu, X., Wang, S.X., Cheng, Z., Xing, J., Zhao, B., Wang, J.D., and Hao, J.M.: Source, transport

736   and impacts of a heavy dust event in the Yangtze River Delta, China, in 2011, Atmos. Chem.

737   Phys., 14, 1239–1254, doi:10.5194/acp-14-1239-2014, 2014.

738   García, O. E., Díaz, J. P., Expósito, F. J., Díaz, A. M., Dubovik, O., Dubuisson, P., Roger, J.-C.,

739   Eck, T. F., Sinyuk, A., Derimian, Y., Dutton, E. G., Schafer, J. S., Holben, B. N., and

740   García, C. A: Validation of AERONET estimates of atmospheric solar fluxes and aerosol

741 radiative forcing by ground-based broadband measurements, J. Geophys. Res., 113, D21207,

742 doi:10.1029/2008JD010211, 2008.

743 García, O. E., Díaz, J. P., Expósito, F. J., Díaz, A. M., Dubovik, O., and Derimian, Y.: Aerosol

744 radiative forcing: AERONET based estimates, climate Models, edited by: Druyan, L., ISBN:

745 978-953-51-0135-2, InTech, 2012.

746 Giles, D. M., Holben, B. N., Tripathi, S. N., Eck, T. F., Newcomb, W. W., Slutsker, I., Dickerson,
747 R. R., Thompson, A. M., Mattoo, S., and Wang, S. H.: Aerosol properties over the
748 Indo-Gangetic Plain: A mesoscale perspective from the TIGERZ experiment, Journal of
749 Geophysical Research Atmospheres, 116, 10--1029, 2011.

750 Giles, D. M., Holben, B. N., Eck, T. F., Sinyuk, A., Smirnov, A., Slutsker, I., Dickerson, R. R.,

751 Thompson, A. M., and Schafer, J. S.: An analysis of AERONET aerosol absorption properties

752 and classifications representative of aerosol source regions, Journal of Geophysical Research

753 Atmospheres, 117, 127-135, 2012.

754 Goloub, P., Li, Z., Dubovik, O., Blarel, L., Podvin, T., Jankowiak, I., Lecoq, R., Deroo, C.,

755 Chatenet, B., and Morel, J. P.: PHOTONS/AERONET sunphotometer network overview:

756 description, activities, results, Fourteenth International Symposium on Atmospheric and Ocean

757 Optics/Atmospheric Physics, 69360V-69360V-69315, 2007.

758 Hansen, J., Sato, M., Ruedy, R., Lacis, A., and Oinas, V.: Global warming in the twenty-first
759 century: an alternative scenario, Proc. Nat. Acad. Sci. USA, 97, 9875-9880, 2000.

760 Haywood, J.M., and Shine, K.P.: The effect of anthropogenic sulfate and soot aerosol on the

761 clear sky planetary radiation budget, Geophys. Res. Lett., 22, 603-606, DOI:

762 10.1029/95GL00075, 1995.

763 He, Q., Li, C., Geng, F., Yang, H., Li, P., Li, T., Liu, D., and Pei, Z.: Aerosol optical properties

764 retrieved from Sun photometer measurements over Shanghai, China, J. Geophys. Res.

765 Atmos., 117, 81-81, 2012.

766 Holben, B. N., Eck, T. F., Slutsker, I., Tanré, D., Buis, J. P., Setzer, A., Vermote, E., Reagan, J.

767 A., Kaufman, Y. J., Nakajima, T., Lavenu, F., Jankowiak, I., and Smirnov, A.: AERONET—A

768 Federated Instrument Network and Data Archive for Aerosol Characterization, Remote

769 Sensing of Environment, 66, 1-16, https://doi.org/10.1016/S0034-4257(98)00031-5, 1998.

770 Holben, B. N., Tanré, D., Smirnov, A., Eck, T. F., Slutsker, I., Abuhassan, N., Newcomb, W. W.,

771 Schafer, J. S., Chatenet, B., and Lavenu, F.: An emerging ground-based aerosol climatology:

772 Aerosol optical depth from AERONET, J. Geophys. Res. Atmos., 106, 12067–12097, 2001.

773   Holben, B. N., Kim, J., Sano, I., Mukai, S., Eck, T. F., Giles, D. M., Schafer, J. S., Sinyuk, A.,

774   Slutsker, I., Smirnov, A., Sorokin, M., Anderson, B. E., Che, H., Choi, M., Crawford, J. E.,

775   Ferrare, R. A., Garay, M. J., Jeong, U., Kim, M., Kim, W., Knox, N., Li, Z., Lim, H. S., Liu, Y.,

776   Maring, H., Nakata, M., Pickering, K. E., Piketh, S., Redemenn, J., Reid, J. S., Salinas, S., Seo,

777   S., Tan, F., Tripathi, S. N., Toon, O. B., and Xiao, Q.: An overview of meso-scale aerosol

778   processes, comparison and validation studies from DRAGON networks, Atmos. Chem. Phys.

779   Discuss., https://doi.org/10.5194/acp-2016-1182, in review, 2017.

780   Huang, X., Ding, A., Liu, L., Liu, Q., Ding, K., Niu, X., Nie, W., Xu, Z., Chi, X., Wang, M., Sun, J.,

781   Guo, W., and Fu, C.: Effects of aerosol–radiation interaction on precipitation during

782   biomass-burning season in East China, Atmos. Chem. Phys., 16, 10063-10082,

783   doi:10.5194/acp-16-10063-2016, 2016.

784   Intergovernmental Panel on Climate Change (IPCC).Climate Change 2013. The Scientific

785   Basis; Cambridge University Press: New York, NY, USA, 2013.

786   Kaufman, Y. J., Tanré, D., and Boucher, O. A.: satellite view of aerosols in the climate system,

787   Nature, 419, 215–223, 2002.

788   Lacis, A. A., and Oinas, V.: A description of the correlated kdistribution method for modeling

789   nongray gaseous absorption, thermal emission, and multiple scattering in vertically

790   inhomogeneous atmospheres, J. Geophys. Res., 96, 9027–9063, 1991.

791   Lack, D. A., and Cappa, C. D.: Impact of brown and clear carbon on light absorption

792   enhancement, single scatter albedo and absorption wavelength dependence of black carbon,

793   Atmos. Chem. Phys., 10(9), 4207-4220, 2010.

794   Lee, K. H., Li, Z., Cribb, M. C., Liu, J., Wang, L., Zheng, Y., Xia, X., Chen, H., and Li, B.:

795   Aerosol optical depth measurements in eastern China and a new calibration method, J.

796   Geophys. Res., 115, 4038-4044, doi: 10.1029/2009JD012812, 2010.

797   Lee, J., Kim, J., Song, C.H., Kim, S.B., Chun, Y., Sohn, B.J., and Holben, B.N.: Characteristics

798   of aerosol types from AERONET sunphotometer measurements, Atmos. Environ., 44, 3110–

799   3117, http://dx.doi.org/10.1016/j.atmosenv.2010.05.035, 2010.

800   Li, J., Carlson, B. E., and Lacis, A. A.: Using single-scattering albedo spectral curvature to

801   characterize East Asian aerosol mixtures, J. Geophys. Res. Atmos., 120, 2037–2052, 2015a.

802   Li, S., Wang T., Xie M., Han Y., and Zhuang B.: Observed aerosol optical depth and angstrom

803 exponent in urban area of Nanjing, China, Atmos. Environ., 123, 350–356, 2015b.

804 Li, W.J., Shao, L.Y., and Buseck, P.R.: Haze types in Beijing and the influence of agricultural

805 biomass burning, Atmos. Chem. Phys. 10, 8119–8130, 2010.

806 Li, W.J., Sun, J.X., Xu, L., Shi, Z.B., Riemer, N., Sun, Y.L., Fu, P.Q., Zhang, J.C., Lin, Y.T.,

807 Wang, X.F., Shao, L.Y., Chen, J.M., Zhang, X.Y., Wang, Z. F. and Wang, W.X.: A conceptual

808 framework for mixing structures in individual aerosol particles, J. Geophys. Res., 121,

809 13205-13798, doi:10.1002/2016JD025252, 2016.

810 Li, Z.Q., Eck,T., Zhang, Y., Zhang, Y.H., Li, D.H., Li, L., Xu, H., Hou, W.Z., Lv, Y., Goloub, P. and

811 Gu, X.F.: Observations of residual submicron fine aerosol particles related to cloud and fog

812 processing during a major pollution event in Beijing, Atmos. Environ., 86, 187–192, 2014.

813 Li Z., Lau, W.K.-M., Ramanathan,V., Wu,G., Ding,Y., Manoj,M.G., Liu,J., Qian,Y., Li,J., Zhou,T.,

814 Fan,J., Rosenfeld,D., Ming,Y., Wang,Y., Huang,J., Wang,B., Xu,X., Lee,S.-S., Cribb,M.,

815 Zhang,F., Yang,X.,Takemura, Wang,K., Xia,X., Yin,Y., Zhang,H.,Guo,J.,Zhai,P.M.,

816 Sugimoto,N.,Babu,S. S., and Brasseur,G.P.: Aerosol and monsoon climate interactions over

817 Asia, Rev. Geophys., doi:10.1002/2015RG000500, 2016.

818 Liu, Q.,Ding, W.D.,Xie, L.,Zhang, J.Q.,Zhu, J.,Xia, X.A.,Liu, D.Y.,Yuan, R.M., and Fu, Y.F.:

819 Aerosol properties over an urban site in central East China derived from ground

820 sun-photometer measurements, Sci. China Earth Sci., 60, 297–314,doi:

821 10.1007/s11430-016-0104-3, 2017.

822 Myhre, G.: Consistency between satellite-derived and modeled estimates of the direct aerosol

823 effect, Science, 325, 187–190, 2009

824 Nakajima, T., and Tanaka, M.: Algorithms for radiative intensity calculations in moderately thick

825 atmospheres using a truncation approximation, J. Quant. Spectrosc. Radiat. Transfer, 40, 51–

826 69, 1988.

827 Pan, L., Che, H., Geng, F., Xia, X., Wang, Y., Zhu, C., Chen,M., Gao,W., and Guo, J.: Aerosol

828 optical properties based on ground measurements over the Chinese Yangtze Delta Region,

829 Atmos. Environ., 44(21), 2587-2596, 2010.

830 Panicker, A.S., Lee, D.I., Kumkar, Y.V., Kim, D., Maki, M., Uyeda, H.: Decadal climatological

831 trends of aerosoloptical parameters over three different environments in South Korea., Int. J.

832 Climatol., 33, 1909–1916, 2013.

833   Pappalardo, G., Amodeo, A., Apituley, A., Comeron, A., Freudenthaler, V., Linné, H., Ansmann,

834   A., Bösenberg, J., D'Amico, G., Mattis, I. Mona, L., Wandinger, U., Amiridis,V.,

835   Alados-Arboledas, L., Nicolae, D., and Wiegner, W.: EARLINET: Towards an advanced

836   sustainable European aerosol Lidar network, Atmos. Meas. Tech., 7, 2389–2409, 2014.

837   Roger, J.-C., Mallet, M., Dubuisson, P., Cachier, H., Vermote, E., Dubovik, O., and Despiau, S.:

838   A synergetic approach for estimating the local direct aerosol forcing:applications to an urban

839   zone during the ESCOMPTE experiment, J. Geophys. Res., 111, D13208,

840   http://dx.doi.org/10.1029/2005JD006361, 2006.

841   Russell, P.B., Bergstrom, R.W., Shinozuka, Y., Clarke, A.D., DeCarlo, P.F., Jimenez, J.L.,

842   Livingston, J.M., Redemann, J., Dubovik, O., and Strawa, A.: Absorption Angstrom exponent

843   in AERONET and related data as an indicator of aerosol composition, Atmos.Chem. Phys., 10,

844   1155–1169, http://dx.doi.org/10.5194/acp-10-1155-2010, 2010.

845   Saha, A., and Moorthy, K. K.: Impact of precipitation on aerosol spectral optical depth and

846   retrieved size distributions: A case study, Journal of Applied Meteorology, 43, 902-914, 2004.

847   Sanap, S.D., and Pandithurai, G.: Inter-annual variability of aerosols and its relationship with
848   regional climate over Indian subcontinent, Int. J. Climatol., 35, 1041–1053,
849   http://dx.doi.org/10.1002/joc.4037, 2014.

850   Schwartz, S.E., and Andreae, M.O.: Uncertainty in climate change caused by aerosols,

851   Science, 272, 1121–1122, 1996.

852   Shen X. J., Sun, J. Y., Zhang, X. Y., Zhang, Y. M., Zhang L., Che, H. C., Ma, Q. L., Yu, X. M.,
853   Yue, Y. and Zhang, Y. W.: Characterization of submicron aerosols and effect on visibility during
854   a severe haze-fog episode in Yangtze River Delta, China, Atmospheric Environment, 120,
855   307-316, 2015.

856   Smirnov, A., Holben, B.N., Eck, T.F., Dubovik, O., and Slutsker, I.: Cloud screening and quality

857   control algorithmsfor the AERONET data base, Remote Sens. Environ., 73, 337–349, 2000.

858   Smirnov, A., Holben, B. N., Lyapustin, A., Slutsker, I., and Eck, T. F.: AERONET processing

859   algorithms refinement, AERONET Workshop, May 10– 14, 2004, El Arenosillo, Spain, 2004.

860   Sokolik, I. N., and Toon, O. B.: Incorporation of mineralogical composition into models of the

861   radiative properties of mineral aerosol from UV to IR wavelengths, J. Geophys. Res., 104(D8),

862   9423-9444, doi:10.1029/ 1998JD200048, 1999.

863   Solomon, S., Qin, D., Manning, M., Chen, Z., Marquis, M., Averyt, K.B.,Tignor, M., Miller, and

864   H.L.(Eds.): Climate change 2007: the physical science basis., Contribution of Working Group I

to the Fourth Assessment Report of the Intergovernmental Panel on Climate Change. Cambridge University Press, Cambridge, United Kingdom and New York, USA, 2007.

Stamnes, K., Tsay, S.C., Wiscombe, W., and Jayaweera, K.: Numerically stable algorithm for discrete-ordinate-method radiative transfer in multiple scattering and emitting layered media, Appl. Opt., 27, 2502–2509, 1988.

Sun, Y., Sun, X., Yin, Y., and Han, Y.: Observation Study of Aerosol over Mid-Western North China Plain in Autumn (October), Plateau Meteorology, 32, 1308-1320, 10.7522/j.issn.1000-0534.2012.00123, 2013 (in Chinese).

Sun, T., Che, H., Qi, B., Wang, Y., Dong, Y., Xia, X., Wang, H., Gui, K., Zheng, Y., Zhao, H., Ma, Q., Du, R., and Zhang, X.: Aerosol optical characteristics and their vertical distributions under enhanced haze pollution events: effect of the regional transport of different aerosol types over eastern China, Atmos. Chem. Phys. Discuss., https://doi.org/10.5194/acp-2017-805, 2017.

Takamura, T., and Nakajima, T.: Overview of SKYNET and its activities, Opt. Puray. Apl., 37, 3303–3308, 2004.

Tan, H., Wu, D., Deng, X., Bi, X., Li, F., and Deng, T.: Observation of aerosol optical depth over the Pearl River Delta, Acta Sci. Circum., 29, 1146–1155, 2009 (in Chinese).

Twomey, S.A., Piepgrass, M., and Wolfe, T.L.: An assessment of the impact of pollution on the global cloud albedo, Tellus., 36B, 356-366, 1984.

Wang, L.C., Gong, W., Xia, X.A., Zhu, J., Li, J., and Zhu, Z.M.: Long-term observations of aerosol optical properties at Wuhan, an urban site in Central China, Atmos. Environ.,101, 94–102, 2015.

Wang, P., Che, H.Z., Zhang, X.C., Song, Q.L., Wang, Y.Q., Zhang, Z.H., Dai, X., and Yu, D.J.: Aerosol opticalproperties of regional background atmosphere in Northeast China, Atmos. Environ., 44, 4404–4412, 2010.

Wang, S., and Zhang, C.: Spatial and temporal distribution of air pollutant emissions from open burning of crop residues in China, Sciencepaper Online, 3, 329–333, 2008 (in Chinese).

Wang, Z., Liu, D., Wang, Y., Wang, Z., and Shi, G.: Diurnal aerosol variations do affect daily averaged radiative forcing under heavy aerosol loading observed in Hefei, China, Atmos. Meas. Tech., 8, 2901, 2015.

Wehrli, C.: Calibration of filter radiometers for the GAW Aerosol Optical Depth network at

895 Jungfraujoch and Mauna Loa. In: Proceedings of ARJ Workshop, SANW Congress, Davos,

896 Switzerland, pp. 70-71,2002.

897 Xia, X., Chen, H., Goloub, P., Zong, X., Zhang, W., and Wang, P.: Climatological aspects of

898 aerosol opticalproperties in North China Plain based on ground and satellite remote-sensing

899 data, J. Quant. Spectrosc. Radiat.Transf., 127, 12–23, 2013.

900 Xia, X., Li, Z., Holben, B., Wang, P., Eck, T., Chen, H., Cribb, M., and Zhao, Y.: Aerosol

901 optical properties and radiative effects in the Yangtze Delta region of China, J. Geophys. Res.,

902 112, D22S12, doi:10.1029/2007JD008859, 2007.

903 Xia, X., Che, H., Zhu, J., Chen, H., Cong, Z., Deng, X., Fan, X., Fu, Y., Goloub, P., Jiang, H.,

904 Liu, Q., Mai, B., Wang, P., Wu, Y., Zhang, J., Zhang, R., and Zhang, X.: Ground-based remote

905 sensing of aerosol climatology in China: Aerosol optical properties, direct radiative effect and

906 its parameterization, Atmos. Environ., 124, Part B, 243-251, 2016,

907 https://doi.org/10.1016/j.atmosenv.2015.05.071.

908 Xie, Y., Zhang, Y., Xiong, X.X, Qu, J.J., and Che, H.Z.: Validation of MODIS aerosol optical

909 depth product over China using CARSNET measurements, Atmos. Environ., 45, 5970-5978,

910 2011.

911 Xin, J., Wang, Y., Li, Z., Wang, P., Hao, W., Nordgren, B., Wang, S., Liu, G., Wang, L., Wen, T.,

912 Sun, Y., and Hu, B.: Aerosoloptical depth (AOD) and angstrom exponent of aerosols observed

913 by the Chinese Sun Hazemeter Networkfrom August 2004 to September 2005, J. Geophys.

914 Res., 112 (D05203), 2007.

915 Xin, J.Y., Zhang, Q., Gong, C.S., Wang, Y.S., Du, W.P., and Zhao, Y.F.: Aerosol direct radiative

916 forcing over Shandong Peninsula in East Asia from 2004 to 2011, Atmos. Ocean. Sci. Lett., 7,

917 74-79, 2014.

918 Xu, X., and Wang, J.: Retrieval of aerosol microphysical properties from AERONET

919 photopolarimetric measurements: 1. Information content analysis, J. Geophys. Res. Atmos.,

920 120, 7059–7078, doi:10.1002/2015JD023108, 2015.

921 Xu, X., Wang, J., Zeng, J., Spurr, R., Liu, X., Dubovik, D., Li L., Li, Z., Mishchenko, M.I., Siniuk,

922 A., and Holben B.N.: Retrieval of aerosol microphysical properties from AERONET

923 photopolarimetric measurements: 2. A new research algorithm and case demonstration, J.

924 Geophys. Res. Atmos., 120, 7079–7098, doi:10.1002/2015JD023113, 2015.

925 Yang, M., Howell, S.G., Zhuang, J., and Huebert, B.J.: Attribution of aerosol light absorption to

926 black carbon, brown carbon, and dust in China – interpretations of atmospheric measurements

927 during EAST-AIRE, Atmos. Chem. Phys., 9, 2035–2050,

928 http://www.atmos-chem-phys.net/9/2035/2009/, doi:10.5194/acp-9-2035-2009, 2009.

929 Zhang, L., Sun, J. Y., Shen, X. J., Zhang, Y. M., Che, H., Ma, Q. L., Zhang, Y. W., Zhang, X. Y.,

930 and Ogren, J. A.: Observations of relative humidity effects on aerosol light scattering in the

931 Yangtze River Delta of China, Atmos. Chem. Phys., 15, 8439-8454,

932 doi:10.5194/acp-15-8439-2015, 2015.

933 Zhang, Q., Streets, D., Carmichael, G., He, K., Huo, H., Kannari, A., Klimont, Z., Park, I.S.,
934 Reddy, S., Fu, J., Chen, D., Duan, L., Lei, Y., Wang, L., and Yao, Z.L.: Asian emissions in 2006
935 for the NASA INTEX-B mission, Atmos. Chem. Phys., 9,5131-5153,
936 doi:10.5194/acp-9-5131-2009, 2009.

937 Zhang, X., Wang, Y., Niu, T., Zhang, X., Gong, S., Zhang, Y., and Sun, J.: Atmospheric aerosol

938 compositions in China: spatial/temporal variability, chemical signature, regional haze

939 distribution and comparisons with global aerosols. Atmos. Chem. Phys., 12, 779–799,

940 http://dx.doi.org/10.5194/acp-12-779-2012, 2012.

941 Zhao, H., Che, H., Zhang, X., Ma, Y., Wang, Y., Wang, X., Liu, C., Hou, B., and Che, H.:
942 Aerosol optical properties over urban and industrial region of Northeast China by using
943 ground-based sun-photometer measurement, Atmos. Environ., 75, 270–278, 2013.

944 Zhao, H., Che, H., Ma, Y., Xia, X., Wang, Y., Wang, P, and Wu, X.: Temporal variability of the

945 visibility, particulate matter mass concentration and aerosol optical properties over an urban

946 site in Northeast China. Atmos. Res., 166, 204-212, 2015.

947 Zheng, C., Zhao, C., Zhu, Y., Wang, Y., Shi, X., Wu, X., Chen, T., Wu, F., and Qiu, Y.: Analysis
948 of Influential Factors for the Relationship between PM2.5 and AOD in Beijing, Atmos. Chem.
949 Phys. Discuss., https://doi.org/10.5194/acp-2016-1170, in review, 2017.

950 Zhu, J., Che, H., Xia, X., Chen, H.B, Goloub, P., and Zhang, W.: Column-integrated aerosol

951 optical and physical properties at a regional background atmosphere in North China Plain,

952 Atmos. Environ., 84,54–64, 2014.

953 Zhuang, B., Wang, T., Li, S., Liu, J., Talbot, R., Mao, H., Yang, X., Fu, C., Yin, C., Zhu, J., Che,

954 H., and Zhang, X.: Optical properties and radiative forcing of urban aerosols in Nanjing over

955 China, Atmos. Environ., 83, 43–52, 2014.

956 Zhuang, B., Wang, T., Liu, J., Che, H., Han, Y., Fu, Y., Li, S., Xie, M., Li, M., Chen, P., Chen, H.,

957 Y, X., and Sun, J.: The optical, physical properties and direct radiative forcing of urban

958   columnar aerosols in Yangtze River Delta, China, Atmos. Chem. Phys. Discuss.,

959   https://doi.org/10.5194/acp-2017-215, 2017.

960   Figure captions

961   Figure 1. Locations and elevations of the seven CARSNET sites in the Yangtze River Delta.

962   Figure 2.Temporal variations in the aerosol volume-size distributions at (a) Hangzhou, (b)

963   Xiaoshan, (c) Fuyang, (d) LinAn, (e) Tonglu, (f) Jiande and (g) ChunAn.

964   Figure 3. Variations in the total, fine- and coarse-mode $AOD_{440\ nm}$ at (a) Hangzhou, (b)

965   Xiaoshan, (c) Fuyang, (d) LinAn, (e) Tonglu, (f) Jiande and (g) ChunAn. The boxes represent

966   the 25th to 75th percentiles of the distributions while the dots and solid lines within each box

967   represent the means and medians, respectively.

968   Figure 4. Variations in the single scattering albedo at 440, 670, 870, and 1020 nm at (a)

969   Hangzhou, (b) Xiaoshan, (c) Fuyang, (d) LinAn, (e) Tonglu, (f) Jiande and (g) ChunAn. See

970   Figure 3 for an explanation of the symbols.

971   Figure 5. (a) Annual average absorption aerosol optical depths at 440 nm ($AAOD_{440\ nm}$) at the

972   CARSNET sites and month-to-month variations in $AAOD_{440\ nm}$ at (b) Hangzhou, (c) Xiaoshan,

973   (d) Fuyang, (e) LinAn, (f) Tonglu, (g) Jiande and (h) ChunAn. See Figure 3 for an explanation

974   of the symbols.

975   Figure 6. (a) Annual variations of monthly mean direct aerosol radiative forcing (50-80 degrees

976   SZA) at the bottom of the atmosphere over (b) Hangzhou, (c) Xiaoshan, (d) Fuyang, (e) LinAn,

977   (f) Tonglu, (g) Jiande and (h) ChunAn. See Figure 3 for an explanation of the symbols.

978   Figure 7. (a) Annual variations in the monthly mean direct aerosol radiative forcing (50-80

979   degrees SZA) at the top of the atmosphere (TOA) at (b) Hangzhou, (c) Xiaoshan, (d) Fuyang,

980   (e) LinAn, (f) Tonglu, (g) Jiande and (h) ChunAn. See Figure 3 for an explanation of the

981   symbols.

982   Figure 8. The aerosol type classification using SSA as a function of $AE_{440-870\ nm}$ over (a)

983   Hangzhou, (b) Xiaoshan, (c) Fuyang, (d), LinAn, (e) Tonglu, (f) Jiande and (g) ChunAn. See

984   text for description of groups I–VII.

985   Figure 9. The distribution of the aerosol type classification over (a) Hangzhou, (b) Xiaoshan, (c)

986   Fuyang, (d), LinAn, (e) Tonglu, (f) Jiande and (g) ChunAn. See text for description of types I–

987   VII.

988   Fig.01

989

990

991   Fig.02

994   Fig.03

995

996

997 Figure04

998

999

1000   Fig.05

1001

1002

1003

1004   Fig.06

1005

1006

1007   Fig.07

1008

1009

1010   Fig.08
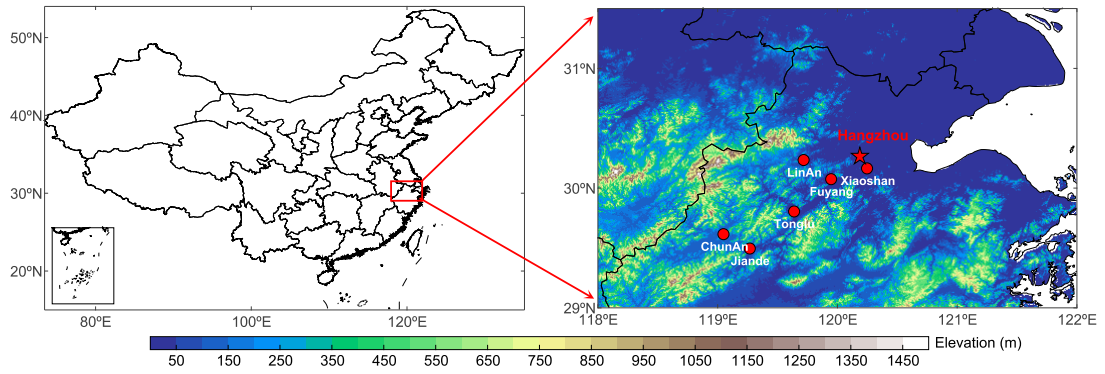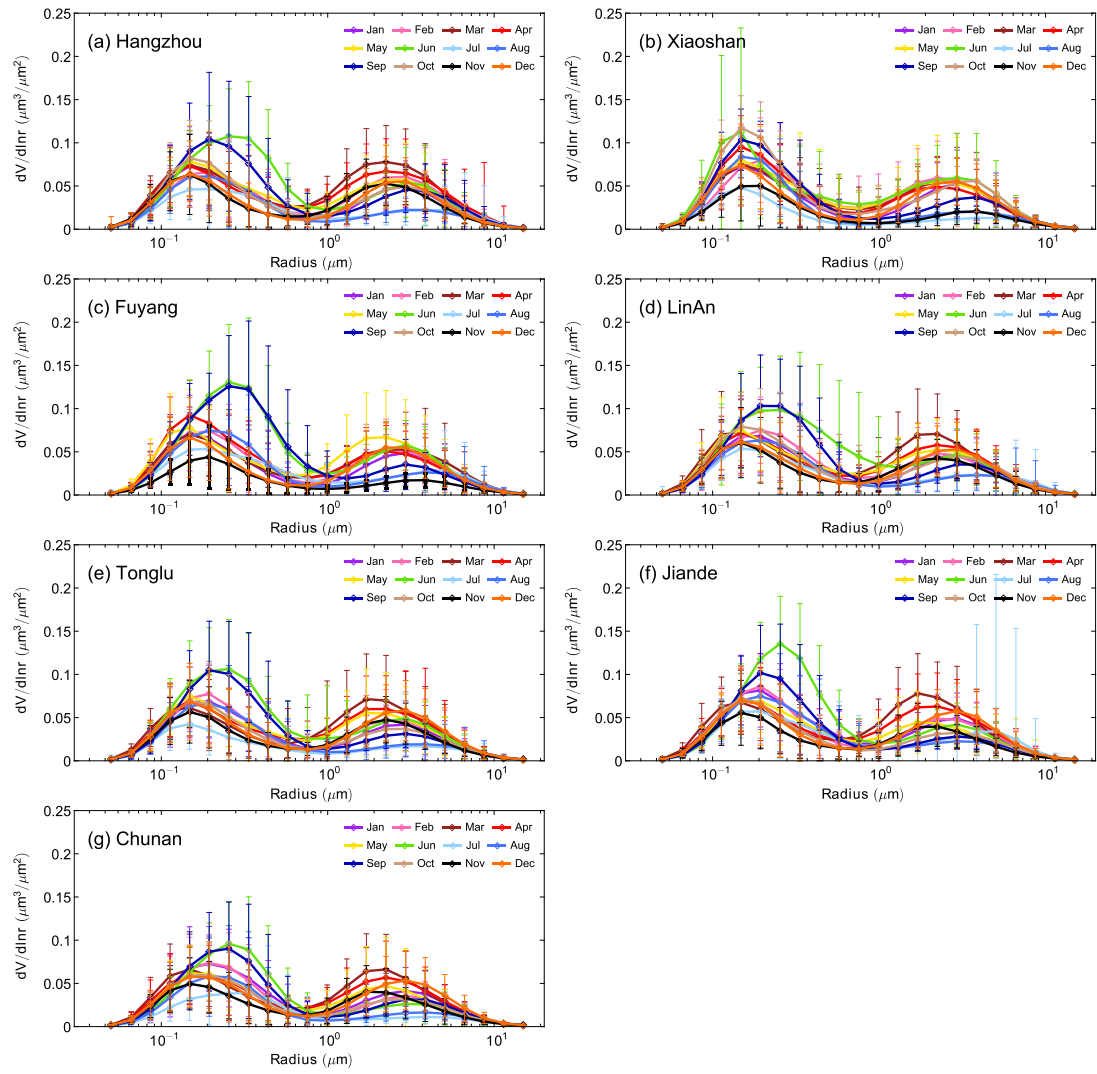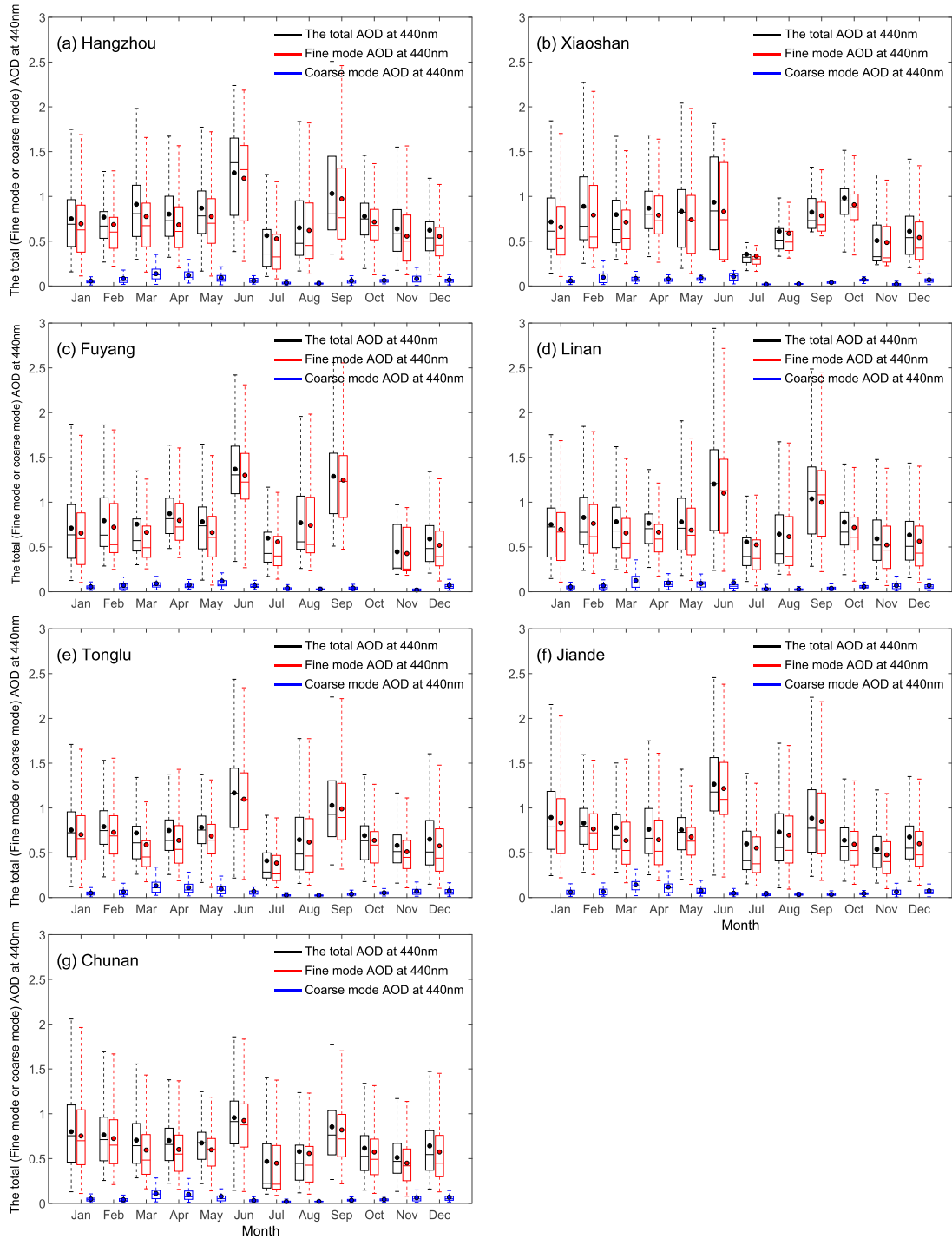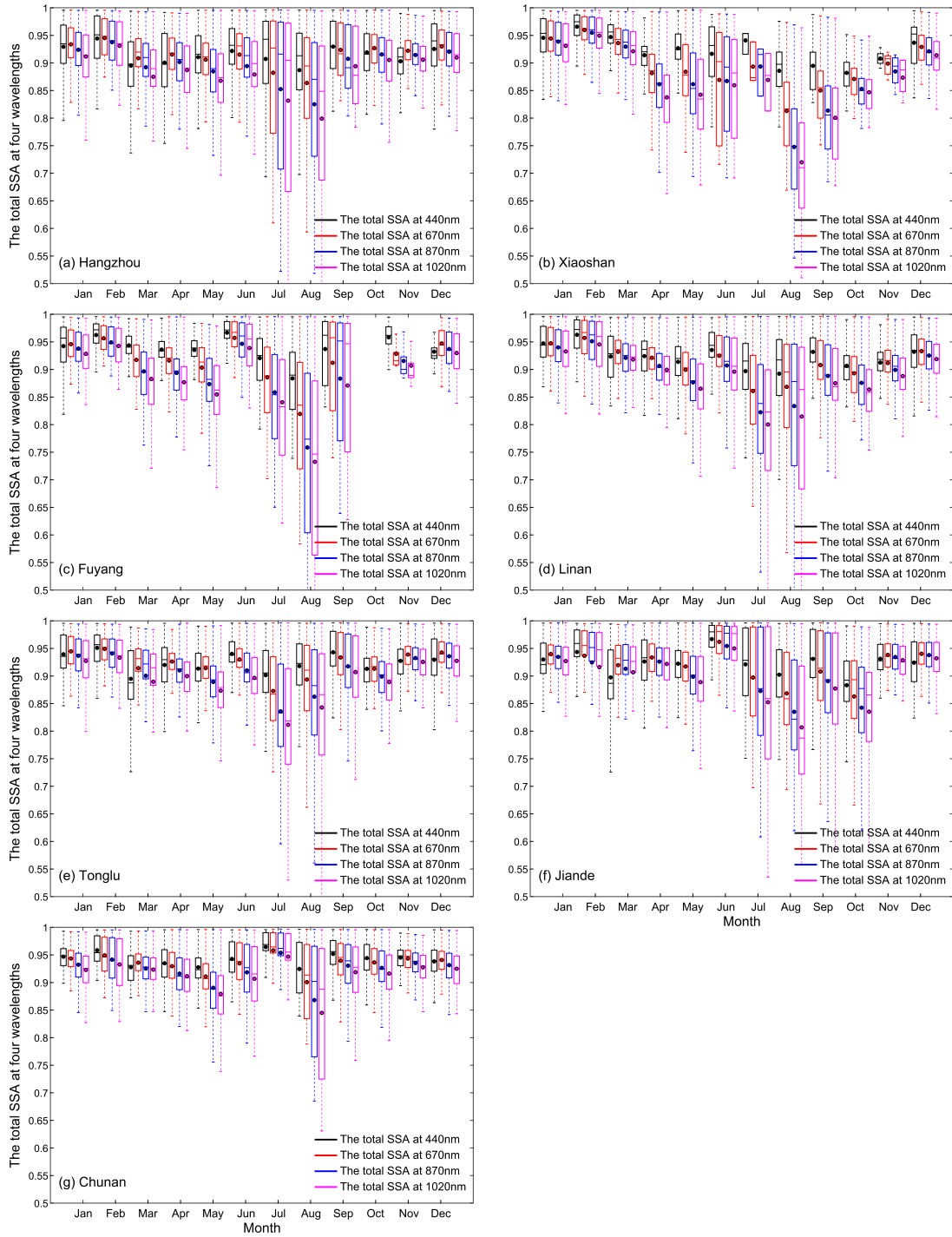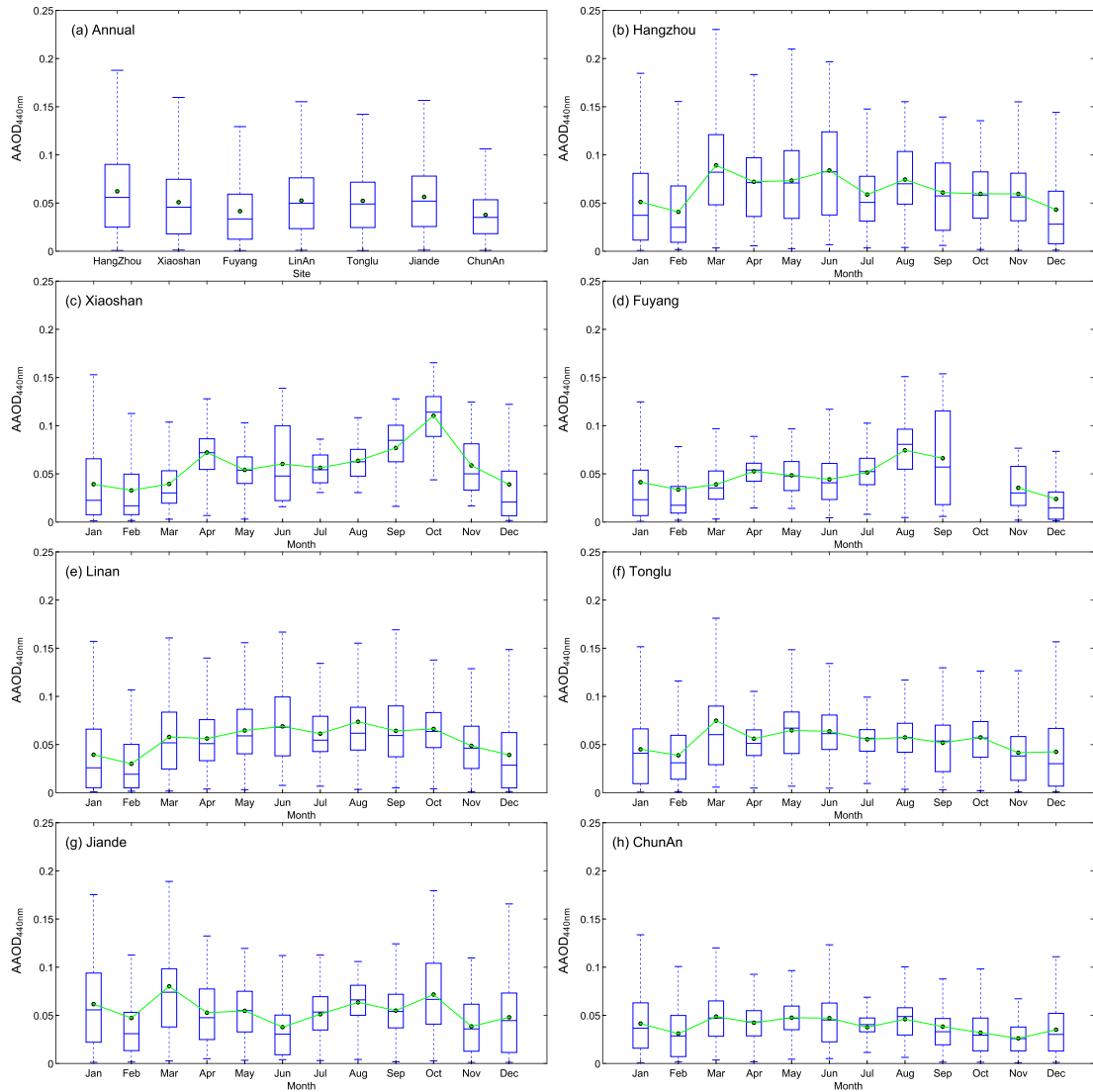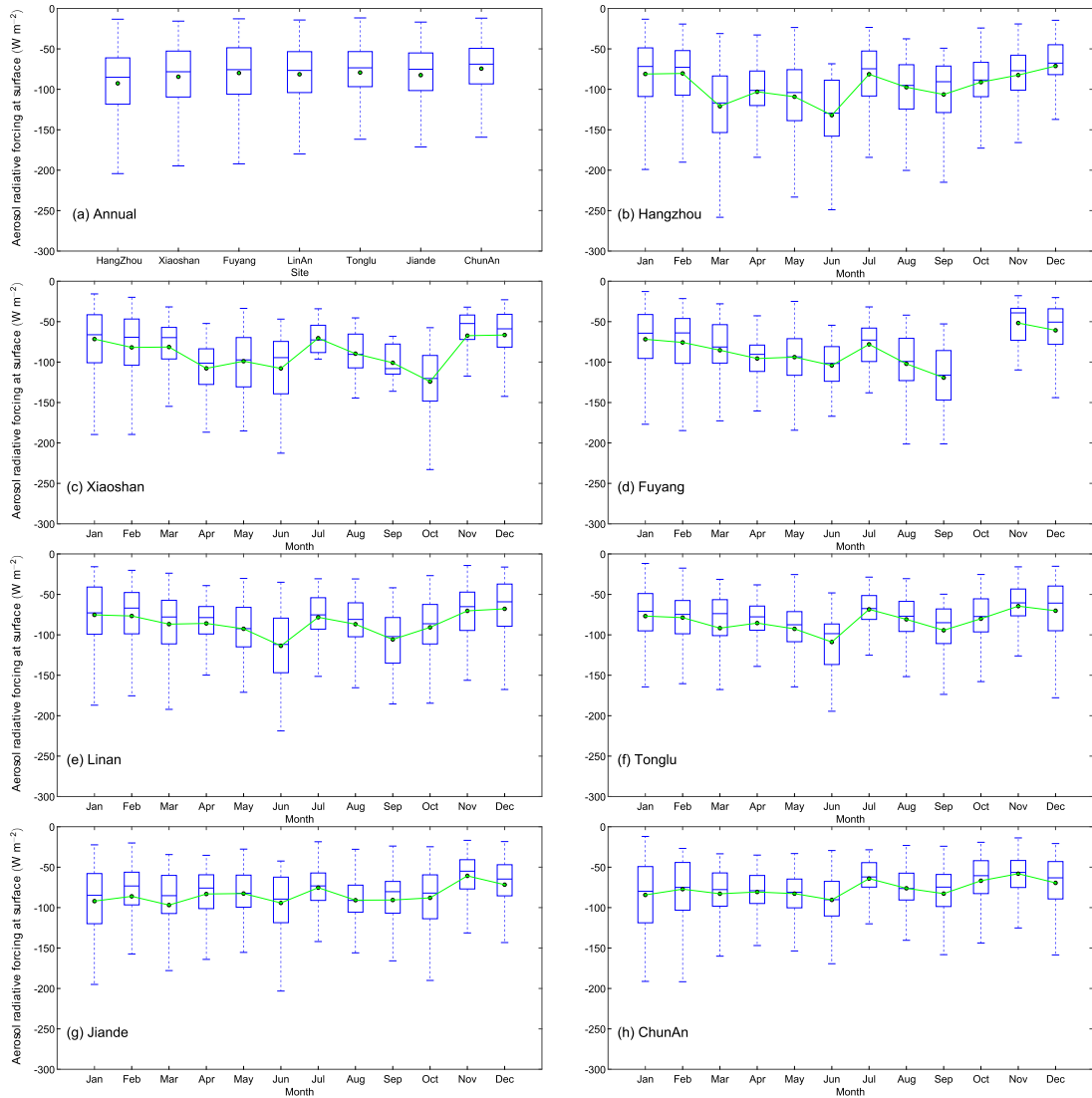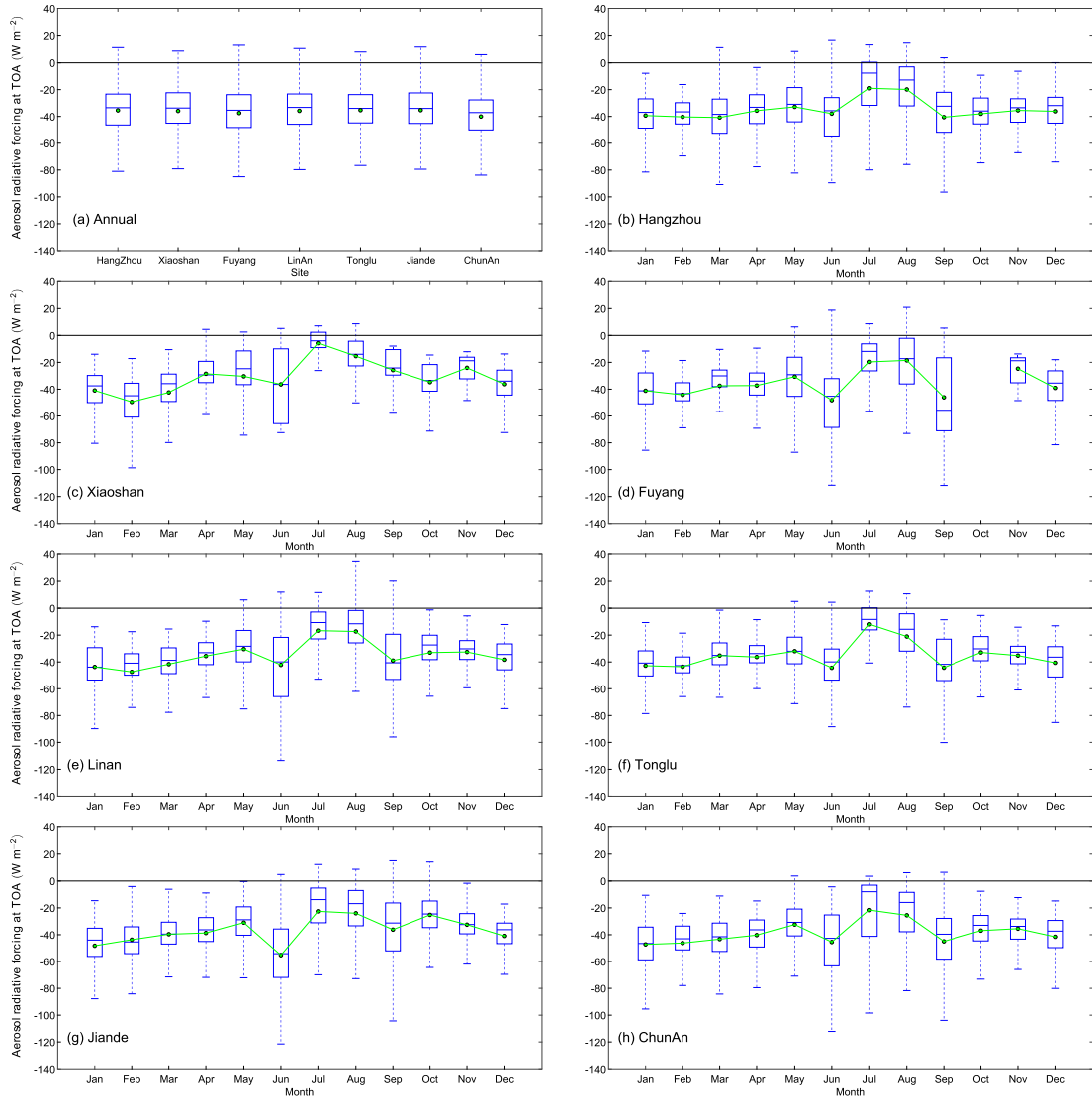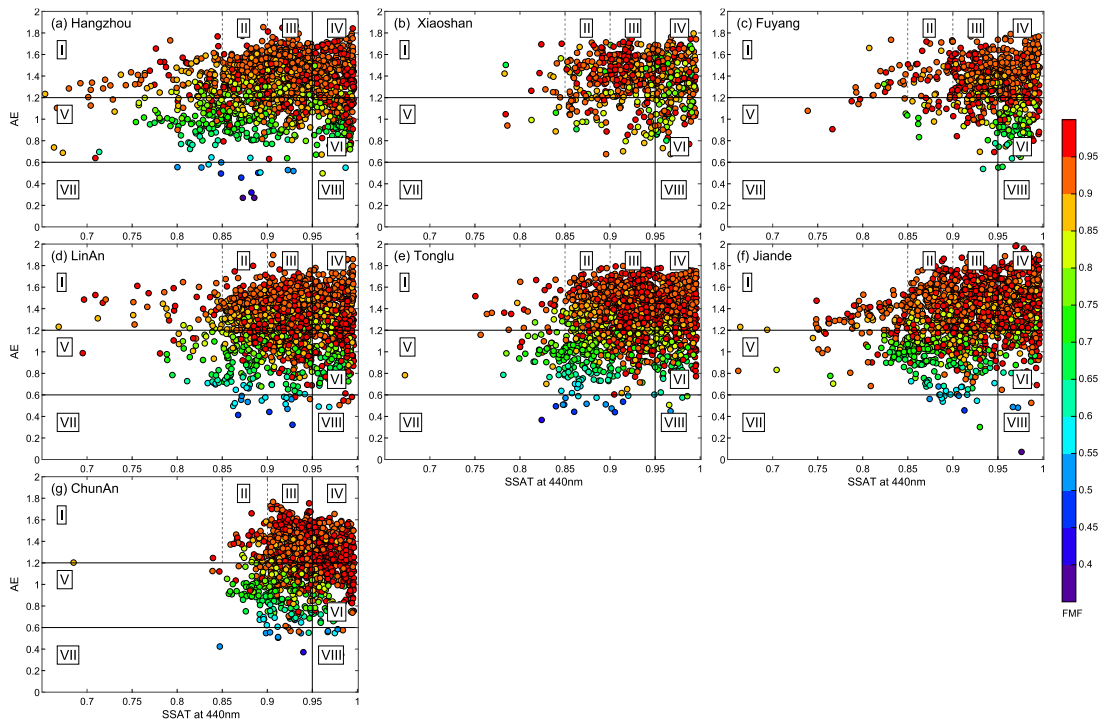
1011

1012

1013 Fig.09

1014

1015

1016   Supplement
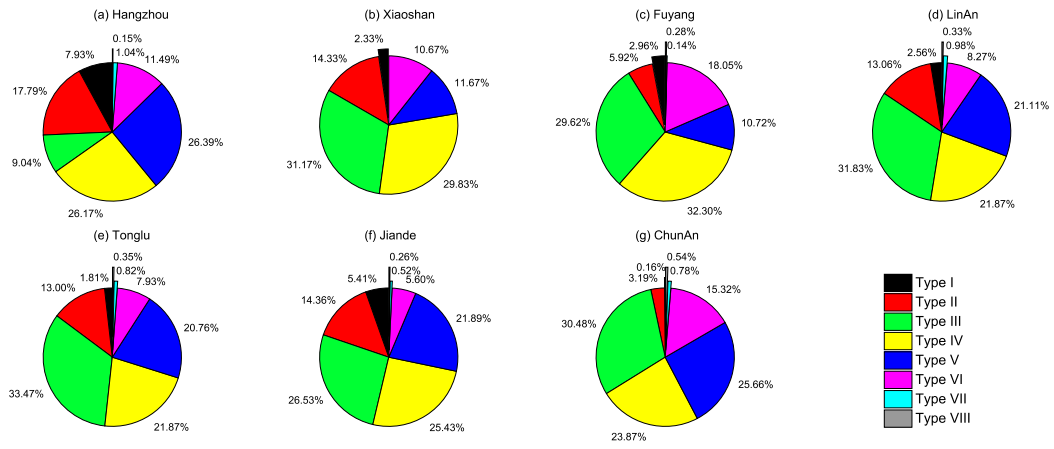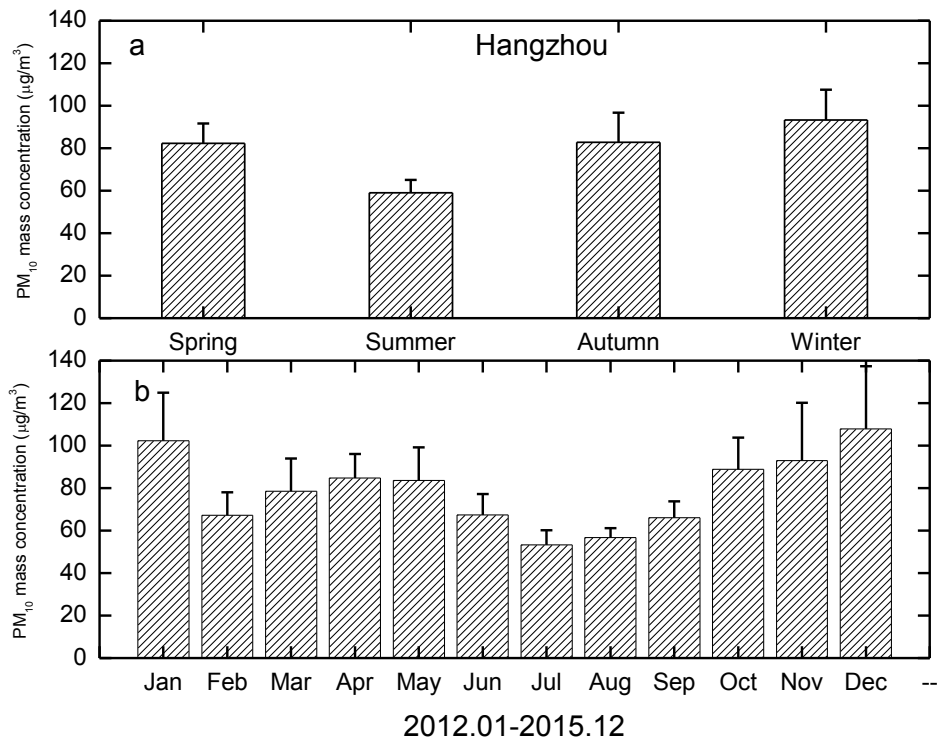
1017

1018   Seasonal and monthly variations of PM10 mass concentrations (μg/m^3) in Hangzhou

1019   during 2012-2015

1020

1021

1022